

Optimal sizing of stand-alone wind-powered seawater reverse osmosis plants without use of massive energy storage

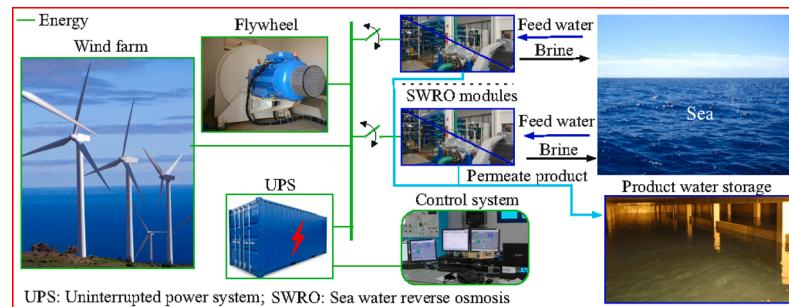
José A. Carta^{*}, Pedro Cabrera

Mechanical Engineering Department, University of Las Palmas de Gran Canaria, Campus de Tafira s/n, 35017, Gran Canaria, Canary Islands, Spain

HIGHLIGHTS

- A method for the optimal sizing of wind-powered desalination plants is proposed.
- The method uses a water storage reservoir and discards use of bulk energy storage.
- A machine learning technique is used to estimate the interannual wind energy.
- The method uses genetic algorithms for the selection of the system components.
- Modules operate under constant conditions or varying their parameters in a range.

GRAPHICAL ABSTRACT



ARTICLE INFO

Keywords:

Wind energy
Water-energy nexus
Desalination
Water storage reservoir
Measure-correlate-predict
Specific costs

ABSTRACT

A method, which involves genetic algorithms, is presented for the optimal sizing of a system comprising a medium-scale modular seawater reverse osmosis desalination plant powered exclusively by off-grid wind energy. The system uses a water storage reservoir that allows coverage of a particular hourly freshwater demand. The use of massive energy storage devices is discarded, although flywheels are used as a dynamic regulation subsystem as well as an uninterrupted power device to supply energy to the control subsystem. The method considers the interannual variation of wind energy, for which it uses machine learning techniques, and introduces randomness in the daily freshwater demand profile. The control strategy is based on ensuring that the energy consumption of the desalination modules remains in synchrony with wind generation throughout the system's useful life, either operating under constant pressure and flow conditions or varying these parameters within an acceptable range. The proposed method is applied to a case study, aiming to cover a freshwater demand of $1825 \times 10^3 \text{ m}^3/\text{year}$, which is equivalent to the water production of a desalination plant with a $5000 \text{ m}^3/\text{day}$ capacity. As the proposed method evaluates the influence of diverse economic and technical parameters, it constitutes a useful tool in the design and implementation of such systems. The results obtained with the optimal system of the case study are compared with those obtained on the basis of a configuration that uses backup batteries to ensure continuous operation. It is shown that the variable operating strategy provides the optimal economic system.

^{*} Corresponding author.

E-mail address: jcarta@dim.ulpgc.es (J.A. Carta).

<https://doi.org/10.1016/j.apenergy.2021.117888>

Received 23 June 2021; Received in revised form 10 August 2021; Accepted 12 September 2021

0306-2619/© 2021 The Author(s). Published by Elsevier Ltd. This is an open access article under the CC BY-NC-ND license

(<http://creativecommons.org/licenses/by-nc-nd/4.0/>).

1. Introduction

The growing demand in many parts of the planet for freshwater for human consumption and agricultural use has led to a substantial increase over the last four decades in the number of desalination plants in use [1], particularly those that use reverse osmosis (RO) technology [2]. The energy sources used to date to power the various desalination technologies that have been developed have predominantly been fossil fuel based. On islands with freshwater scarcity problems and a strong external energy dependence, as in the Canary Islands [3], tackling the different aspects related to the water-energy nexus – which according to Dai *et al.* [4] has become an area of growing interest over the past decade for the scientific and political communities – acquires even greater relevance. This is especially true when, as underlined by Padrón *et al.* [5], the scarcity of freshwater in an area happens to coincide with a significant abundance of renewable energy sources. Roggenburg *et al.* [6] showed the feasibility of the use of RO desalination plants, sized to meet a public freshwater demand of approximately 3.79 Mm³/day for the American side of the US-Mexico border, through an offshore wind farm and an onshore photovoltaic (PV) farm, at a cost of between 2.00 and 3.52 \$/m³. The same authors also highlighted the significant reductions in CO₂ emissions that using such renewable energy sources entails.

Wind is one of the most commonly used renewable energy sources [7], mainly due to the degree of maturity of the technologies associated with its exploitation [8]. Ghaffour *et al.* [7] argued that wind energy-based desalination could be one of the most promising options for seawater desalination, especially in coastal areas with high wind energy potential. González *et al.* [8] described the numerous and highly diverse operating systems and strategies that have been proposed for wind energy powered desalination plants and suggest what the future trends of these systems will be. The owners of the large- and medium-scale desalination plants that have been implemented to date have commonly opted for the installation of wind farms (WFs) and the connection of both subsystems to conventional power distribution grids [8]. However, as pointed out by Segurado *et al.* [9], the integration of wind energy powered desalination into the conventional grid of isolated islands may be limited even in the case of high wind energy potential.

1.1. Literature review on microgrids for water desalination using renewable energies

The wind energy powered desalination systems that have been developed to date to overcome the aforementioned drawback [9] and provide potable water for remote coastal areas where no conventional grid is available are, in effect, stand-alone microgrids. One of the problems in the use of wind power in desalination applications is the variable nature of wind. For this reason, most of the microgrids that have been built have required the incorporation of energy storage systems, mainly batteries [10], or have operated in conjunction with diesel generation systems [11].

Generally, the models proposed in the literature to size microgrids for water desalination using renewable energies have considered connection to the national grid [12] or the use of backup batteries, without [13] or with diesel generators [14], to ensure the continuous operation of the system. Kyriakarakos and Papadakis [15] investigated combinations of small-scale desalination systems using RO technology capable of producing up to a few thousand m³ of desalinated water per day in combination with photovoltaic and wind energy systems in scenarios of both grid connection and stand-alone mode. According to Kyriakarakos and Papadakis [15], the results obtained show that RO desalination, together with renewable energies, can profitably tackle current problems of water scarcity whilst at the same time minimizing the environmental footprint of the process. Very few of the models that have been proposed in the literature have focussed on the study of medium- or large-scale RO desalination plants [16]. To determine the

optimum size of a hybrid renewable energy system, commercial software applications like HOMER which apply a mono-objective optimization are commonly used [17]. Some studies have used particle swarm optimization [15], some have analysed the use of evolutionary algorithms [18], and others have combined the use of HOMER and genetic algorithms [13]. These works fundamentally employ cost-based optimization criteria, but none of them consider the replacement of energy backup systems with systems combining water storage with a new management strategy of the electricity demand of the RO desalination plant, as is proposed in the present study. Unlike the approach that is followed here, RO desalination units are normally considered working at their nominal operating point. However, Kyriakarakos *et al.* [19] reported that a considerable increase in potable water production can be achieved with a variable operating load. According to Gude [20], bearing in mind the mismatch between supply source and demand and the intermittent nature of renewable energy resources, energy storage is an indispensable element for the continuous and reliable operation of desalination facilities. Aboelmaaref *et al.* [21] highlighted the urgent need for the implementation of renewable energies in desalination processes to reduce the negative effect of global warming. In their study, Moazeni *et al.* [22] optimized a micro water-energy system and concluded that the incorporation of batteries decreases the contribution of fossil fuel based energy in the water-energy nexus and reduces CO₂ emissions. However, according to McManus [23], batteries may be manufactured with materials that themselves have a high environmental cost and some of which, such as lithium, are resources in relatively short supply. They therefore stress that increasing dependency on battery-based energy storage systems can have a harmful impact. According to Soshinskaya *et al.* [24], a 100% renewable system would require an extremely large battery storage system which is presently economically unfeasible. In cases where the topographic characteristics are suitable, methodologies have also been proposed to optimize the size and operational strategy of wind-powered desalination and pumped hydro storage systems [9].

González *et al.* [8], in their description of small-, medium- and large-scale off-grid wind energy systems for desalination, carried out an up-to-date worldwide review of projects which have been developed and put into operation at all scales and without the use of massive energy storage devices. Carta *et al.* [25] described a desalination system installed on the island of Gran Canaria (Spain) called the Seawater Desalination with an Autonomous Wind Energy System (SDAWES). The main aim of the SDAWES project, which was designed for fully autonomous operation and use in medium- and large-scale seawater desalination, was to determine the operational viability of using the energy generated by an off-grid WF to power three types of desalination technology without the use of massive energy storage devices. Subiela *et al.* [26] published the lessons that had been learnt after two years of tests performed with the RO, mechanical vapour compression and reverse electro dialysis technologies used within the framework of the SDAWES project. According to Subiela *et al.* [26], the most suitable process was RO, principally due to the rapid start-up. Among the problems detected with the change of phase technology (mechanical vapour compression) Subiela *et al.* [26] highlighted the slowness of the start-up and the generation of calcareous deposits (CaCO₃) which took place after long periods of inactivity of the unit (more than 24 h). As a result of these deposits, laborious maintenance work was required. Carta *et al.* [27] presented an operational analysis of the SDAWES system with the desalination plant comprising eight RO modules. The SDAWES project [27] takes advantage of the modular nature of RO plants, connecting and disconnecting modules which operate under constant pressure and flow conditions, with the aim of ensuring that the variation in energy demand for desalination is in synchrony with the wind generation. As reported by the authors [27], the WF was able to supply the energy needs of the RO modules throughout the entire desalination process (from seawater pumping to product water storage), as well as the energy needs of the control subsystems, without the use of massive energy storage devices. Carta *et al.*

[28] presented a seawater reverse osmosis (SWRO) prototype plant that was designed to continuously adapt its energy consumption to the variable power supplied by a wind turbine (WT), while dispensing with the use of massive energy storage systems. In the prototype described by Carta *et al.* [28], the control system manages the number of pressure vessels that are connected/disconnected from the system and regulates their operating pressures and flows within predetermined acceptable limits in order to maintain a constant permeate recovery rate.

In [27], the technical operational viability of the system developed in the SDAWES project is demonstrated. Nonetheless, this system, for various reasons which the authors indicate in the aforementioned paper, was not designed to optimally cover, from a technical and economic perspective, a particular hourly freshwater demand.

The review of the literature that the authors of the present study have undertaken found that methods have been proposed that aim to analyse the performance of medium- and large-scale SWRO desalination plants that use wind-sourced electrical energy. They follow to a certain degree the operational concept of the SDAWES project. However, Cabrera *et al.* [29] did not contemplate the use of a water storage reservoir (WSR) to allow coverage of a given freshwater demand at all times of the year due to the variability of the wind resource. The simulation that was performed by [30] also did not consider the use of a WSR and did not take into account the interannual variation of this resource, and no information was provided about the cost of the product water. Loutatidou *et al.* [31] proposed the strategic storage of sufficient amounts of freshwater for use in the case of catastrophic events or for long-term supply. However, in their study [31], it is also supposed that conventional grid electricity is available to allow continuous operation of the SWRO plant when the wind energy falls below a minimum established load. Calise *et al.* [32], as in [31], proposed the use of water storage systems to avoid the use of electric ones. However, their proposed microgrid, which is configured with PV panels, is connected to the main electrical grid. That is, the microgrid they considered will operate in on-grid mode, with the main objective of the system they proposed being to reduce electricity exchanges with the main grid using a hydrographic basin as an energy storage system.

1.2. Aim, novelty and key contributions of this paper

One of the reasons for initiating the research study presented here was the observation that a significant number of the methods proposed for the sizing of stand-alone microgrids for water desalination turn to the use of batteries to resolve the problem of variability that is inherent to renewable systems. The solution adopted in the scientific literature generally consists of maintaining constant operation of the desalination plants (at rated operating conditions) even though the energy supply varies with time. This approach results in designs that are heavily dependant on large battery systems to balance important mismatches between demand and generation. However, such designs have various drawbacks, as reported by McManus [23] and Soshinskaya *et al.* [24]. Another of the reasons for undertaking the research study presented here was that, although the technical operational viability of the design has previously and uniquely been demonstrated in [27], the design was not optimized, from a technical and economic perspective, as in this study. The authors therefore concluded that it would be opportune to propose an optimal design method for these systems, taking advantage of the practical experience they have acquired in their design, development and testing.

The main contribution of the method proposed in this research is that the optimization of stand-alone microgrids for water desalination is obtained avoiding the use of massive energy storage systems, like batteries. This is due to the combination of water storage management and the proposal of a novel system control strategy to synchronize the energy consumption of the SWRO modules with wind renewable generation. The aim of this paper is therefore to present a method for the optimal economic sizing of a system comprising a medium-scale modular SWRO

plant -powered exclusively by off-grid wind energy- and a WSR that allows coverage of a particular freshwater demand without the use of massive energy storage devices. However, also forming part of the system are a flywheel energy subsystem (FES) and an uninterrupted power system (UPS). The purpose of the FES is, among others [27], to act as a voltage and frequency reference of the stand-alone electrical grid and to maintain dynamic stability in the face of disturbances. The purpose of the UPS is to supply energy to the control system (central and local of each subsystem) and to ensure the power required by various devices of the WT (yaw mechanism, blade-pitch control, etc.) is covered in periods when insufficient wind power is available or during the minutes prior to WT connection.

The novelty of this paper lies in the fact that it is the first time that a method, which involves genetic algorithms, has been developed in which the system control strategy is to ensure that energy consumption of the SWRO modules is in synchrony with wind generation, whether working under constant pressure and flow conditions (as in the SDAWES system [27]) or when varying these operating parameters within an acceptable range such that the concentration of the product water is constant. In addition, the proposed method introduces randomness in the daily freshwater demand profile and considers the interannual variation of wind energy. For this latter purpose, the method uses measure-correlate-predict (MCP) models [33] based on machine learning techniques whose efficacy has been demonstrated in the estimation of solar radiation time series [34] and, according to Karasu *et al.* [35] and Altan *et al.* [36], in the estimation of wind speed time series. This approach differs substantially from the standard approaches found in the literature, which use a time series that covers just a single year [30] and purely deterministic methods.

The method selects the optimal number of WTs (considering different rated powers) and SWRO desalination modules (considering diverse nominal daily production capacities), the optimal WSR size, and the optimal volume of water that the WSR must contain before the system can be started up. The proposed method also allows determination of the capacities of the UPS and FES that are required for the proper functioning of the system. A discussion is offered of the results obtained from the application of this method to a case study with the objective of covering an annual freshwater demand of $1825 \times 10^3 \text{ m}^3$. The results obtained with the optimal system are then compared with those obtained with a reference system that uses backup batteries to ensure the continuous operation of the SWRO plant.

2. Method

In this section, a description is first provided of the general configuration of the system considered in the method presented in this paper and of the system used as reference system. Following this, the various tasks are developed that comprise the algorithm of the method for the optimal sizing and simulation of medium-scale wind powered modular SWRO plants.

- Description of the general configuration of the system

Fig. 1 provides a rough schematic outline of the general configuration of the proposed system. On the left can be seen the electrical generation subsystem.

The WF will comprise one or more WTs (represented in Fig. 1 by NWT). As mentioned in Section 1.2, an FES and UPS also form part of the electrical generation subsystem.

The loads subsystem comprises an SWRO desalination plant made up of a number (represented in Fig. 1 by Nm) of single-stage SWRO module loads (with 'positive feed-forward' control [37]) fitted with energy recovery devices (ERDs). Each module will have a freshwater production capacity of $Qm \text{ (m}^3 \text{ day}^{-1}\text{)}$ when operating under constant feed pressure $p_f \text{ (Pa)}$ and flow $Q_f \text{ (m}^3 \text{ /h)}$ conditions. Likewise, each module, operating with a recovery rate of $Y \text{ (%)}$ will have a mean production of $Q_p \text{ (m}^3 \text{ /h)}$

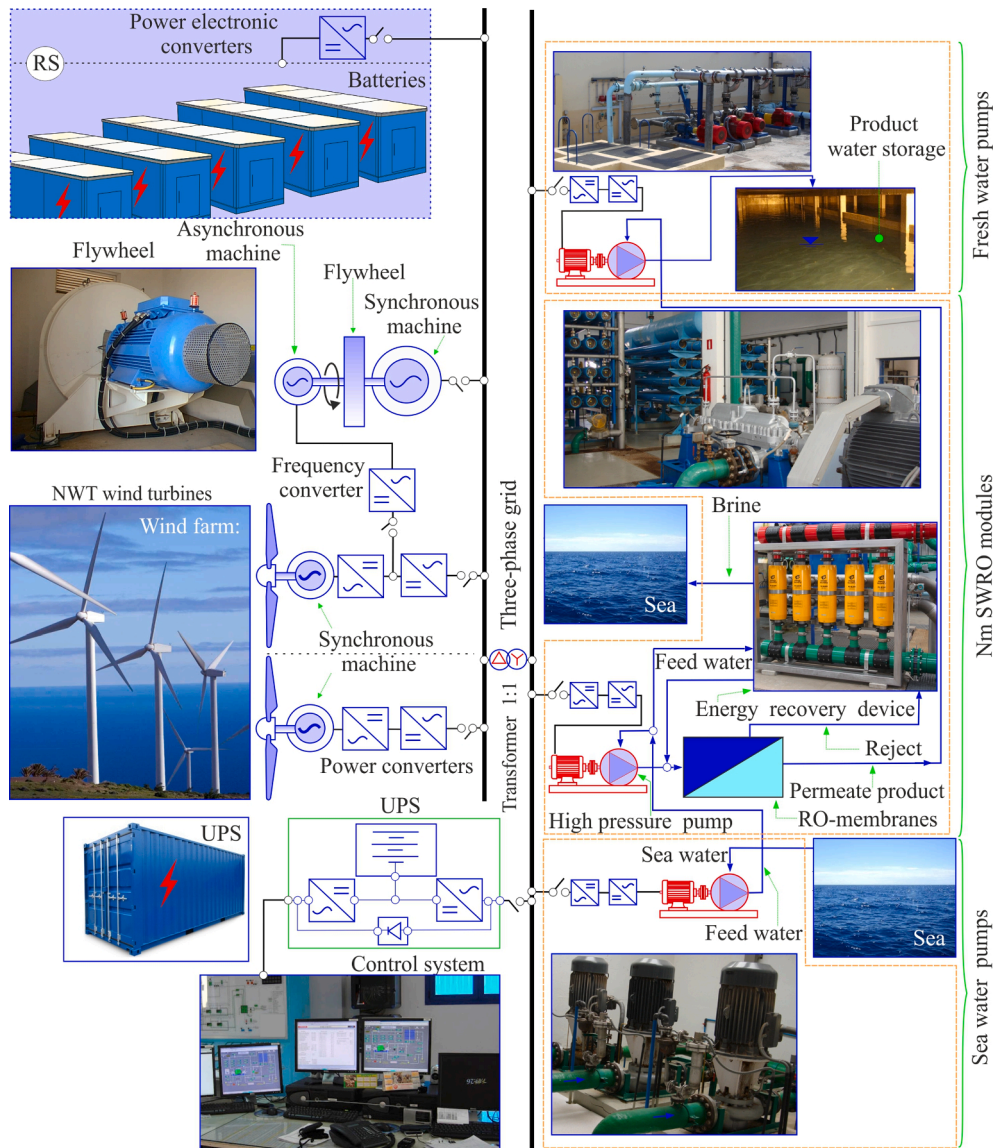


Fig. 1. Representative outline of the configuration of the system.

with a product water concentration of C_p (mg/L) and a specific energy consumption of C_e (kWh per cubic metre of product water) in which the energy consumption of the feed and freshwater pumps is included.

The freshwater pump subsystem includes a WSR, with a capacity of V_s (m^3), which requires an initial water volume of V_o (m^3) before the system is put into operation in order to avoid the seasonal variability of the wind impeding permanent coverage throughout the year of the hourly freshwater demand.

The transformer represented in Fig. 1 has a 1:1 ratio and is connected in triangle/star form, as in the case of the SDAWES project [27]. This transformer is used for protection for homopolar faults on the secondary side (if one phase goes to earth the current passes through neutral and appropriate protections are activated so that the loads are out of service and the generation remains active).

The basic protocol of the operation of the system considered in the method presented in this paper is described in Carta *et al.* [27]. In this reference, a description can be found of the electrical generation subsystem, the load subsystem and the control subsystem of the SDAWES project. Likewise, the system operation is described, indicating the process for the creation of the isolated electrical grid, the load connection procedure and the strategies in the connection-disconnection order of the SWRO modules. The transformer is connected before start-up and

before the excitation system of the synchronous machine is connected in order to isolate both circuits and avoid excess currents that could damage the equipment [27].

The systems that is used as a reference system, hereinafter referred to as RS, consists of a stand-alone microgrid that comprises a WF and a backup electrochemical energy storage system to ensure the continuous operation of an SWRO plant. The RS also has a WSR to ensure a balance at all times between the water produced by the SWRO plant working under constant operating conditions and the variable water demand. The elements of the electrical generation subsystem that pertain exclusively to the RS are shown in Fig. 1 surrounded by a dashed line and with a circle with the letters ‘RS’.

- Tasks covered by the algorithm of the method.

Fig. 2 shows a block diagram of the set of tasks proposed to select the optimal system, from an economic perspective, which comprises a modular SWRO desalination plant powered by a stand-alone WF and a WSR that allows coverage of a particular hourly freshwater demand and without the use of massive energy storage systems.

The first task in the proposed method is estimation of the long-term wind resource at the target site using an MCP method and the historical

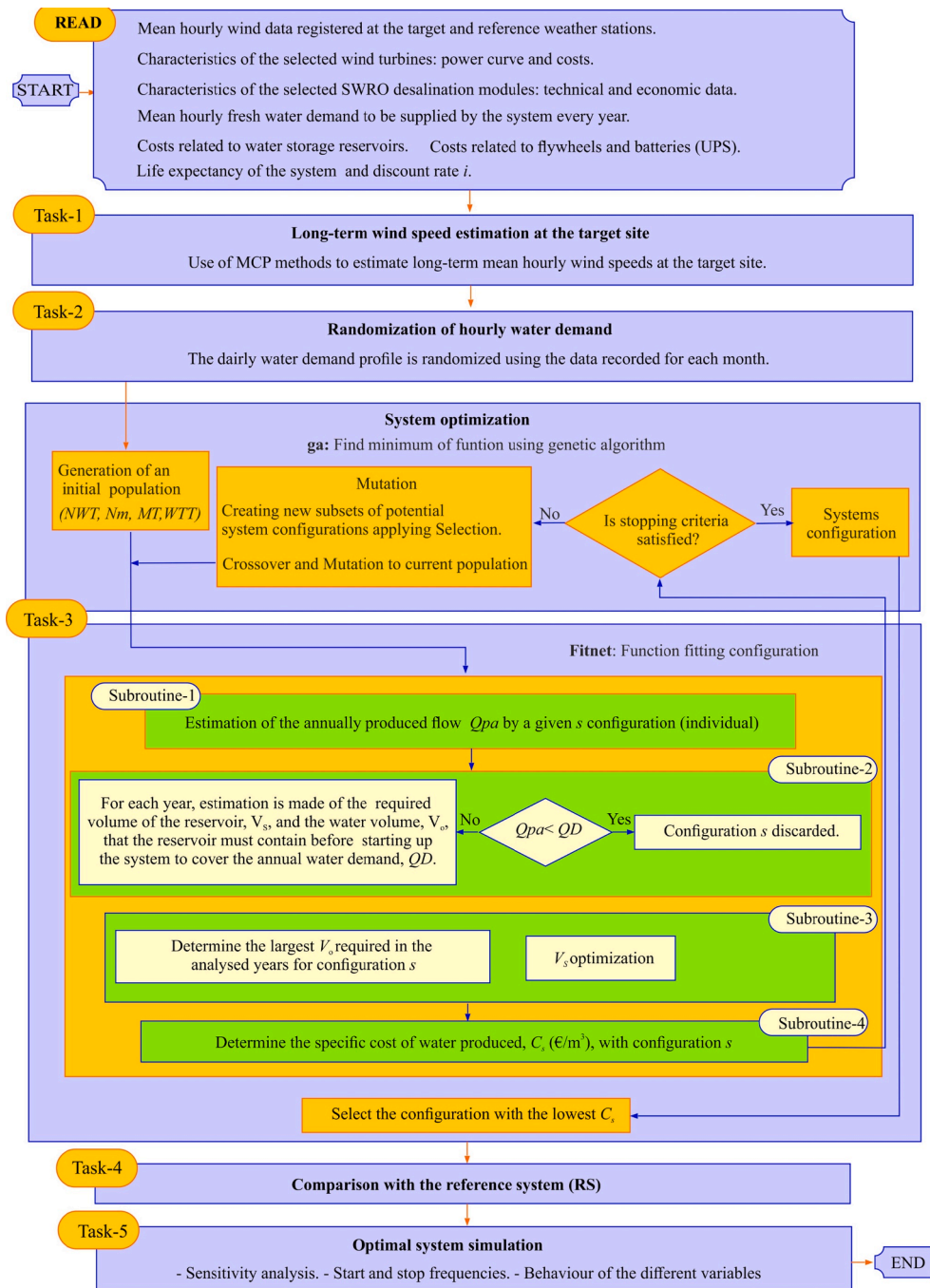


Fig. 2. Block diagram of the tasks proposed for selection of the optimal economic scenario.

data series recorded at the reference weather stations (WSs). This task is developed in Section 2.1.

After estimating the wind resource at the hub height of the WT at the target site corresponding to the years considered in the study, the second task of the process is carried out (Fig. 2). This task consists of the randomization of the profile of the daily freshwater demand that the system aims to cover and is developed in Section 2.2.

The optimization process is undertaken in the third task (Fig. 2). Genetic algorithms (GA) were used to select the NWT for each WT type (WTT) that is considered and the Nm for each of the Qm mean daily freshwater production capacities that are considered. These algorithms were selected for different reasons, including: a) their demonstrated efficacy when the aim is to calculate non-differentiable functions, b) as they are intrinsically parallel, c) they are less affected by local maxima

(false solutions) than traditional techniques, d) they do not require specific knowledge about the problem they are trying to resolve, e) they use probabilistic operators instead of the typical deterministic operators of other techniques, f) they are very easy to execute in modern massive architectures in parallel, g) unlike other more recent stochastic methods, like particle swarm optimization, the conceptual development of GAs has had, since its origins, mathematical backing that supports it, h) the result is highly independent of the initial conditions, i) due to our experience in the use of GAs in the resolution of entire optimization problems [38].

More specifically, the 'ga' function of Matlab's Global Optimization Toolbox [39] was used. This function allows the resolution of entire optimization problems.

The first stage of the optimization process consists of the generation

of an initial population. In this case, the population is comprised of a set of individuals, where each individual represents the set of 'nvars' variables that represent *NWT*, *Nm*, the SWRO module type (*MT*) and *WTT*, and constitutes a possible optimal configuration of the system.

Once this population has been generated, the fitness of each individual has to be evaluated.

This fitness function recognises the technical and economic characteristics assigned to the *WTT* and *MT* variables and is the objective function of the optimization problem in question. The target is to find the system configuration which meets the water demand and at the same time minimizes the product water cost.

Firstly, the objective function analyses for each individual (potential configuration) of the population whether the cumulative annual flow that it can produce, *Qpa*, in each of the wind years considered is able to cover the annual water demand, $\sum_{t=1}^{8760} QD_t$. In the event that a given configuration does not meet this condition, it is discarded (the algorithm of the objective function penalizes this fact by assigning a high cost to the product water).

For the configurations that satisfy the condition in all the analysed years that $Qpa \geq \sum_{t=1}^{8760} QD_t$, an estimation is then made of the reservoir volumes, *Vs*, that are required to cover the mean hourly water demand and of the water volumes, *Vo*, that the reservoir must contain before starting up the system defined by these configurations.

The specific cost, *Cs* (€/m³), of the product water with each of the configurations that have not been discarded is then estimated. For this estimation, the investment and operating and maintenance costs of the subsystems which make up the configurations (WTs, SWRO desalination plant, WSR, UPS and FES) are taken into account, as are the estimated lifetime, *L*, and the discount rate, *i*.

The 'ga' algorithm (Fig. 2) analyses the values *Cs* of each individual (system configuration) and finalizes its execution when the number of iterations has reached the value 'MaxGenerations' = 200 or if the mean relative change in the best fitness function value over 'MaxStallGenerations' is less than or equal to a 'FunctionTolerance' = 10⁻⁴. For as long as the above indicated stop requirements are not met, the 'ga' algorithm generates a new population that is again evaluated. Subsequently, the

genetic operators like the *crossover* -which combines part of the genetic information of its parents- and the *mutation* -which randomly alters the values of some genes in a parental chromosome- are stochastically applied. To obtain integer variables, 'ga' uses special creation, crossover, and mutation functions [40]. The fraction of the population at the next generation, not including elite children, that the crossover function creates was set at 'CrossoverFraction' = 0.8. The number of individuals of a generation that are guaranteed to survive in the following generation was set at 'EliteCount' = 0.05 · 'PopulationSize'. The algorithms for this task are developed in Section 2.3.

In the fourth task, a comparison of the specific cost obtained with the optimal analysed system configuration is compared with the specific cost of the RS. This fourth task is developed in Section 2.4.

In the fifth and final task, a simulation is performed of the configuration that provided the lowest specific cost. In this simulation, a sensitivity analysis is carried out, the frequency of start-ups/shut-downs of the SWRO modules is considered, and the behaviour of different variables is analysed, including the hourly WSR volume, the mean hourly wind energy powers that are not exploited, etc.

2.1. Task-1. Estimation of long-term wind speed at the target site

The procedure normally employed by MCP methods that use multiple reference WSs comprises two stages [33] (Fig. 3).

As reported in [33], in the first stage (indicated by an encircled number "1" in Fig. 3), it is hoped to establish a relationship between the wind data series recorded at the reference sites and the target site for the short-term period that is common to both. For this, the dataset is divided into two subsets. One of the two data subsets, which is given the name *training data*, is used in the learning algorithm of the MCP model. The other subset, given the name *test data*, is used to evaluate the MCP model that is constructed. In this work, this partition between the training and test data was carried out using the statistical technique known as 10-fold cross-validation [33].

Fig. 3 shows, by way of example, the use of three reference WSs (WS-1, WS-2 and WS-3). However, the number of reference WSs can be

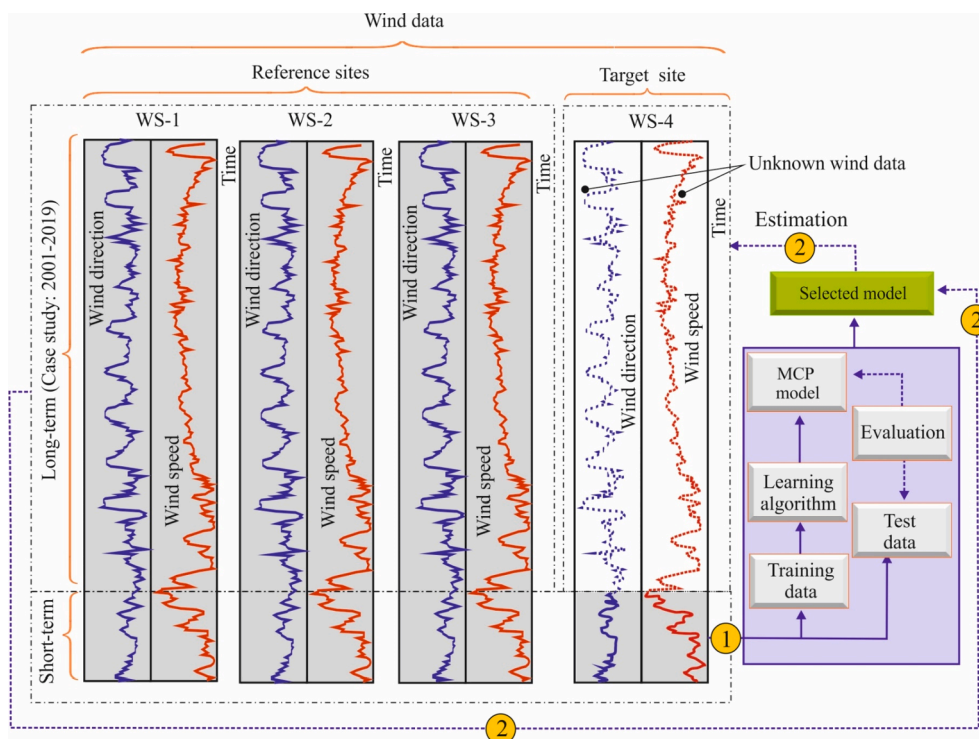


Fig. 3. Block diagram of the procedure normally employed by MCP methods [33].

higher or lower.

In the second stage (indicated by an encircled number “2” in Fig. 3), the long-term wind data series available for the reference WSS are fed into the MCP model selected in stage 1 as input feature. The aim is to undertake an estimation of the historical (or long-term) wind conditions at the target site.

The model M–1 for wind speed estimation uses a multiple regression approach, which is represented in Eq. (1). In the M–1 model proposed in this study, the wind direction signal is introduced using its sine and cosine, and the angle corresponding to the northerly direction is taken as angle 0°.

$$Y_t = f(X_t) = WS - 4(S)_t \\ = f[WS - 1(S)_t, WS - 2(S)_t, WS - 3(S)_t, \cos(WS - 1(D)_t), \sin(WS - 1(D)_t), \cos(WS - 2(D)_t), \sin(WS - 2(D)_t), \cos(WS - 3(D)_t), \sin(WS - 3(D)_t)] \quad (1)$$

In the functional form of the model, $X = (X_1, \dots, X_d)^T$ are the input features, the subscript t indicates the instant evaluated, and $Y_t = WS - 4(S)_t$ represents the estimated output feature or response.

Diverse machine learning techniques have been proposed in the literature to resolve regression function in MCP models. These include artificial neural networks [41], support vector machine [42] and random forest (RF) [43]. In this work, the regression function given in Eq. (1) is estimated using an RF algorithm [44], which has provided adequate results in previous studies conducted by Díaz *et al.* [42] and Cabrera *et al.* [45], and is robust against overfitting [46]. For programming of the RF-based MCP model, the randomForest package [47] of the open-source multi-platform R Statistics software [48] was used. A wrapper technique was used to select the input features of the model analysed, as is usually done with time series prediction models in which diverse input features intervene [49]. The recursive feature elimination (RFE) [50] algorithm, available in the Caret package [51] of the R Statistics software, was used. For more detailed information, please consult the Supplementary Material (S.1: Task-1).

The metrics used to analyse the M–1 model were the mean absolute error (MAE), the index of agreement (IoA) [52], the adjusted coefficient of determination (R_a^2) and the mean squared error (MSE). For more detailed information, please consult the Supplementary Material (S.2: Task-1. The metrics used to analyse the M–1 model).

2.2. Task-2. Randomization, in each month, of the daily freshwater demand profile

This task is based on the assumption of the availability of long-term data of the hourly freshwater demand that it is estimated will be consumed over a year long period.

With this data it is possible to determine seasonal water demand and the mean daily profiles of water demand (red line in Fig. 4) for each of the 12 months of the year.

Given that the optimization method proposed in this work selects the number and capacity of the SWRO modules taking into consideration the differences that can occur in each hour in available wind power and in water demand, it was considered opportune to consider the randomness of the daily freshwater demand profile in addition to the randomness of the wind resource (Task-1).

For this, the time series of hourly data recorded in each of the twelve months of the year is modified with a purpose-built algorithm. Modification of the water demand data series is made for each day of each month and is undertaken in such a way that the mean daily water demand profile of the corresponding month (red line in Fig. 4 which is

shown as an example) is not altered. To achieve this objective, each of the 24-hourly water demand data of a given day and month is randomly (and without replacement) selected from all the data recorded of the hour under consideration during all the days of the month. That is, in the case of Fig. 4, the water demand data corresponding, for example, to 14:00 of each day of the month that Fig. 4 represents come from the random (and without replacement) selection of the data highlighted in the figure by a dashed line box.

2.3. Task-3. System optimization

In this task, the system optimization process represented in Task-3 of

Fig. 2 is carried out. The most representative aspects of the process are differentiated in the subsections below:

2.3.1. Estimation of the initial configurations of the system

In this section, an estimation is carried out of the NWT and N_m for each of the Q_m mean daily freshwater production capacities and WTT that are considered, and which would be required to cover the peak water demand based on the wind data from the year with the least wind power.

These parameters are used to define the initial configurations of the system.

The N_m for each Q_m is determined, Eq. (2), from the value of the peak mean hourly flow ($\max(QD_t)$) which it is estimated will be demanded.

$$N_m = \text{ceiling} \left(\frac{\max(QD_t)}{Q_m/24} \right) \quad (2)$$

where ceiling(\cdot) function returns the smallest integers larger than the parameter.

The power that is required to cover the peak demand with the N_m SWRO modules of Q_m capacity is determined through Eq. (3):

$$P_m = N_m \cdot C_e \cdot \left(\frac{Q_m}{24} \right) \quad (3)$$

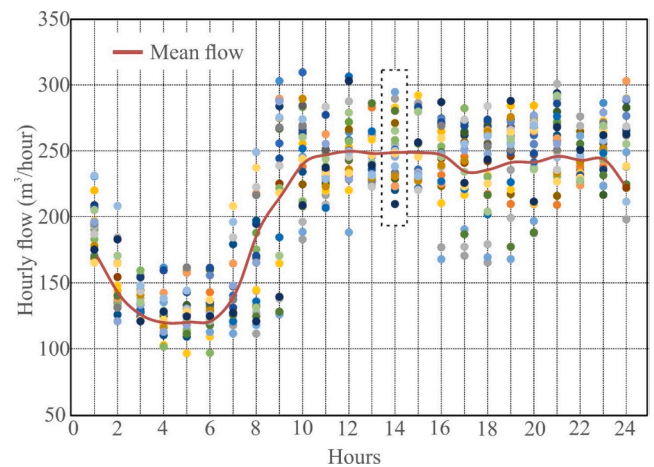


Fig. 4. Example of a mean daily profile of hourly water demand in a particular month. The coloured circles represent the hourly demand data recorded on each day of the month.

The NWT for each WTT which is required to cover P_m is determined through Eq. (4):

$$NWT = \text{ceiling} \left(\frac{P_m}{\overline{WTPO}_{min}} \right) \quad (4)$$

In Eq. (4), \overline{WTPO}_{min} is the smallest mean annual power output that would be obtained with the selected WTT in all the years considered. In this paper, the power curve of the selected WT is used to estimate its power output as a function of the estimated wind speeds (w_s) at its hub height. To estimate the mean hourly WT power output Eq. (5) is used [53]:

$$WTPO_t = \frac{1}{2} c_p \cdot A \cdot \rho \cdot (w_s)^3 \quad (5)$$

where: c_p is the electrical power coefficient of the WT and is a function of the wind speed w_s ; A is the rotor swept area of the WT; and ρ is the air

density at the site where the WT is to be installed.

2.3.2. Generation of the s potential initial system configurations, omitting WSR size

First, a matrix \mathbf{M} , of s rows \times 4 columns, is generated from the parameters estimated in Section 2.3.1, in which each of its rows, without the as yet undefined V_s , represents a potential system configuration. This matrix \mathbf{M} will constitute the 'InitialPopulationMatrix', where the number of rows s will coincide with 'PopulationSize'.

For more detailed information, please consult the Supplementary Material (S.3: Task-3).

2.3.3. Estimation of the cumulative flow that a configuration s of the wind energy powered desalination system is able to produce

Subroutine-1 (Fig. 5) determines the cumulative flow, Q_{pa} , that a given configuration is able to produce annually.

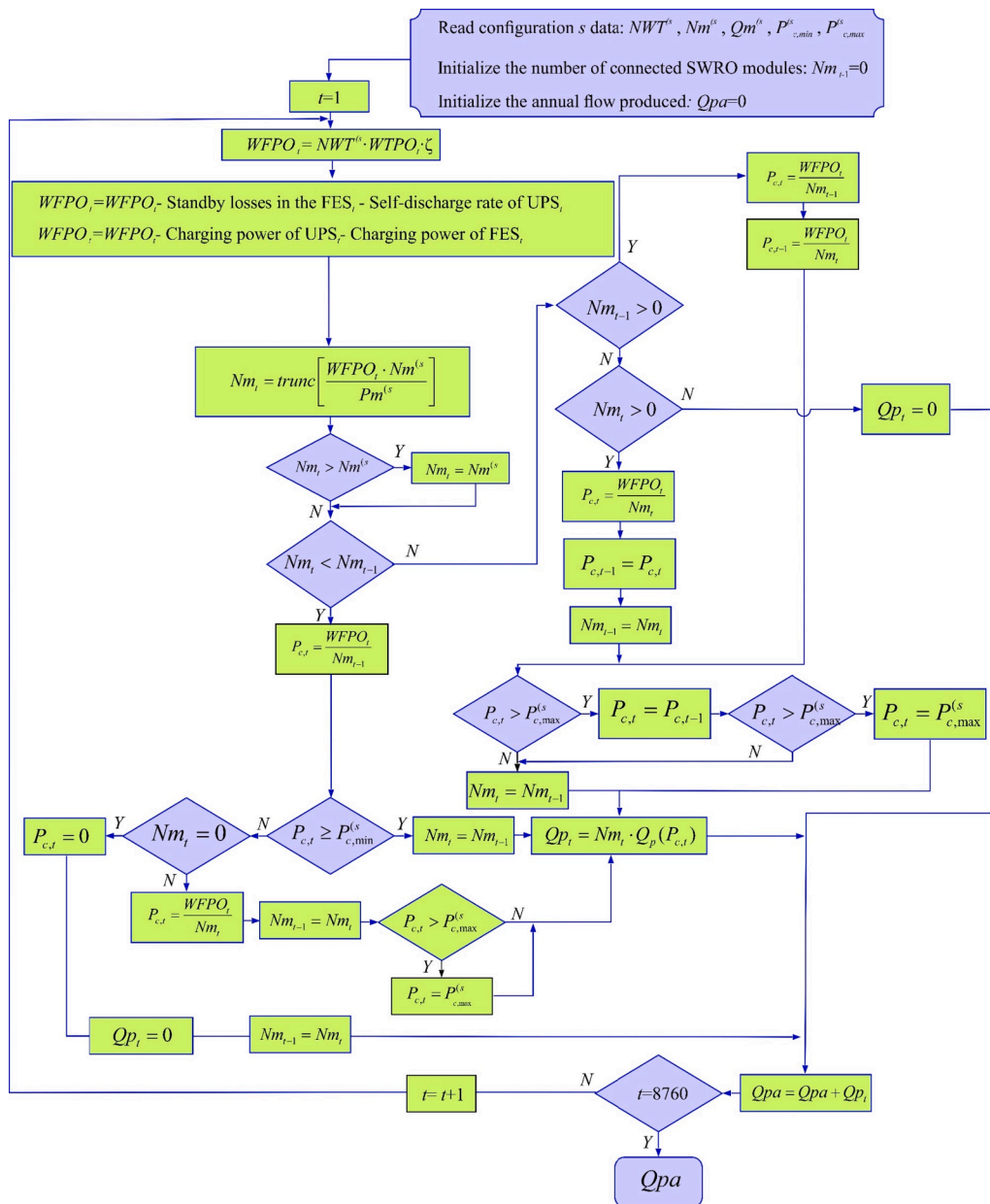


Fig. 5. Subroutine-1. Estimation of the cumulative flow, Q_{pa} , that a given configuration, s , is able to produce annually in the case of the SWRO modules operating under variable pressure and flow conditions.

• Operating strategies of the SWRO modules considered:

Subroutine-1, thus far developed, admits two operating modes of the SWRO modules for energy consumption to be in synchrony with wind generation: a) variable pressure and flow conditions (S-2), such that the concentration of the water product remains constant; and b) constant pressure and flow conditions (S-1), which constitutes a particular case of mode a).

Pohl *et al.* [54] proposed and theoretically analysed diverse operational strategies for the variable operation of SWRO modules, one of which was used by Carta *et al.* [28] in an experimental analysis of a small-scale prototype SWRO desalination plant designed for continuous adjustment of its energy consumption to the widely varying power generated by a stand-alone wind turbine. In the method proposed in the present study, any of the variable operating strategies proposed by Pohl *et al.* [54] can be implemented. However, to date the authors of the present study have only programmed the algorithm which contemplates the strategy of variable pressure and feed flow rate within an acceptable range such that the concentration of the product water remains constant.

In the case of strategy S-2, an analysis is performed in Subroutine-1 at each instant t (one hour) of the series of annual data (8760 data in this work) of the number of SWRO modules, Nm_{t-1} , at the instant $t-1$, in order to decide whether the connection of new modules, the disconnection of one or more modules in operation at $t-1$, or modification of the operating parameters (within an acceptable range) of the modules in operation at $t-1$, is required in order to adapt consumption to the wind energy available at the instant t and thereby decrease the start-up shut-down frequency [46]. The number of modules, Nm_t , which need to be connected at an instant t operating under nominal conditions is determined (Fig. 2) by applying the 'trunc(x)' function to the quotient produced by dividing the power, $WFPO_b$, generated by the WF at that instant t (after covering the loads of the FES and UPS and their energy losses) by the power demand of an SWRO module. trunc(x) takes a single numeric argument x and returns an integer formed by truncating the value in x toward 0. The $WFPO_b$ is determined according to the NWT (number of WTs) that make up the WF, the power output of a WT ($WTPO_i$) with the wind blowing at the instant t , and the estimated efficiency of the WF, ζ , which depends, among other factors, on wake effect losses [53].

The UPS has, in each instant t , to cover the power of the central control unit ($P_{control}$) and of the of the WTs and the SWRO modules ($\tau = 0$), Eq. (6). If there is insufficient wind energy available to cover the power (P_{swt}) demanded by the WTs (yaw mechanism, blade-pitch control, etc.) [55], this power must be covered by the UPS ($\tau = 1$).

$$P_{Batt} = (NWT + Nm + 1) \cdot P_{control} + \tau \cdot NWT \cdot P_{swt} \quad (6)$$

The power P_{FES} , Eq. (7), which the FES must supply will be a percentage ϕ of the power that the Nm modules require at the instant Δt of connection/disconnection. The inertia J of the FES is estimated through Eq. (8) [56]:

$$P_{FES} = \phi \cdot P_m \cdot Nm \rightarrow E_{FES} = P_{FES} \cdot \Delta t \quad (7)$$

$$E_{FES} = \frac{1}{2} \cdot J \cdot (\omega_{max}^2 - \omega_{min}^2) \rightarrow J = \frac{2 \cdot E_{FES}}{(\omega_{max}^2 - \omega_{min}^2)} \quad (8)$$

The power consumed by the FES when increasing the turning speed from ω to ω_{max} is estimated through Eq. (9), which was obtained when resolving the differential equation shown in Eq. (10):

$$P = \frac{\nu \cdot (\omega_{max}^2 \cdot e^{\frac{2\omega \cdot 3600}{J}} - \omega^2)}{e^{\frac{2\omega \cdot 3600}{J}} - 1} \quad (9)$$

$$J \cdot \frac{d\omega}{dt} \omega + \nu \cdot \omega^2 = P \quad (10)$$

The viscous friction coefficient, ν , was estimated through Eq. (11), based on the experience of the authors [27]:

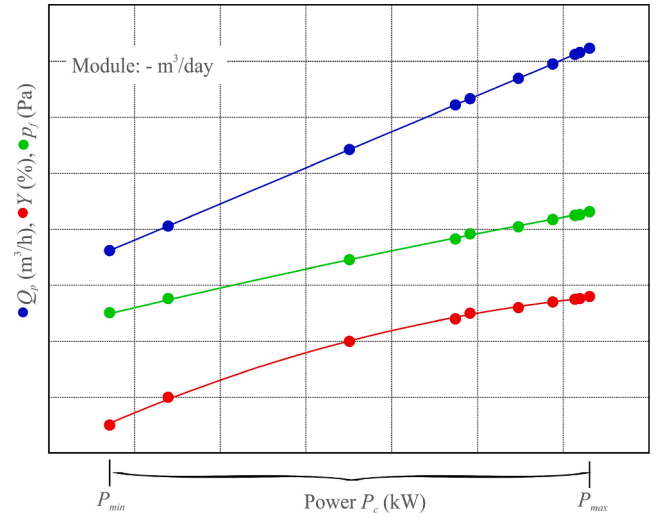


Fig. 6. Representation, by way of example, of the operating variables obtained with a membrane software for a generic SWRO module, within an acceptable operating range, and of the curves fitted to them.

$$\nu = \frac{0.1 \cdot P_{FES} \cdot 1000}{\omega_{max}^2} \quad (11)$$

For each type of SWRO module, estimation is made of the flow, Q_p (m^3/h), that is produced (with a user-defined concentration), the recovery rate and the operating pressure, p_f (Pa), as a function of the power consumed, P_c (kW), within the acceptable operating range of $[P_{min}, P_{max}]$.

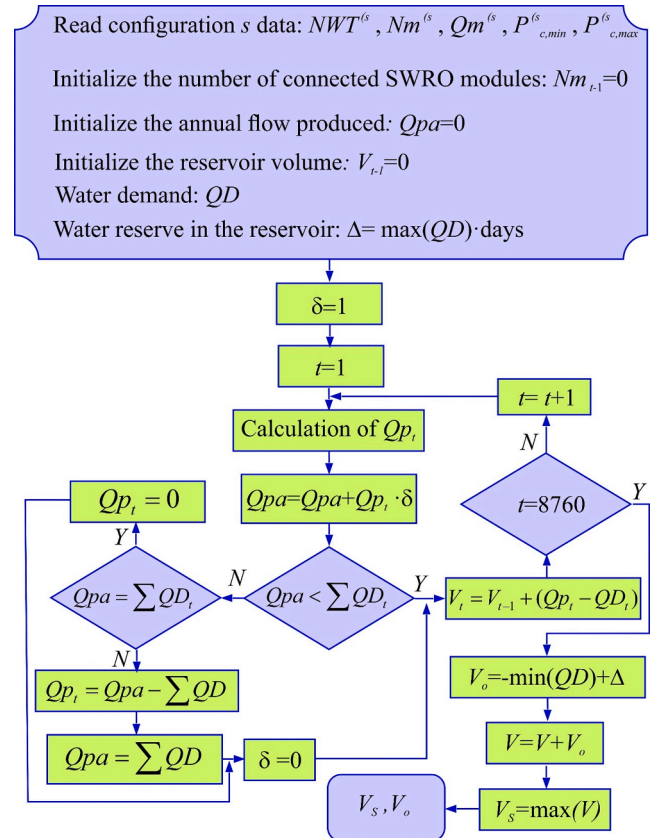


Fig. 7. Subroutine-2. Estimation of the reservoir volume, V_s , and water volume, V_o , required before starting up the system.

These estimations can be obtained with software provided by the membrane manufacturers. In the proposed method they were obtained with the Toray membrane software [57].

Curves are fitted to representative points of the different operating variables obtained for each SWRO module plotted against P_c , Eq. (12). Fig. 6 shows, for a generic model and by way of example, a representation of these operating points obtained with the membrane software used and of the curves fitted to them.

$$\left. \begin{matrix} Q_p (\text{m}^3/\text{h}) \\ Y (\%) \\ p_f (\text{Pa}) \end{matrix} \right\} = \text{function}(P_c) \text{ with } P_c \text{ in kW} \quad (12)$$

2.3.4. Estimation of WSR capacity and initial reservoir volume required to cover water demand

Subroutine-2 (Fig. 7) determines the volumes, V_s and V_o , required to cover freshwater demand. A procedure similar to that employed in Subroutine-1 is used to estimate the flows, $Q_{p,t}$, produced at each instant t .

Depending on the wind power evolution of each year and on that year's water demand, it may occur that the cumulative flow, Q_{pa} , required to cover the annual demand, $\sum_{t=1}^{8760} QD_t$, is reached one or more months before the end of the year, and the system will cease being operational. However, to cover the freshwater demand for the remaining month/s of the year a significantly large-sized WSR may be required (Fig. 8). In order to reduce the volume, V_s , of the WSR, and therefore the investment costs required for its construction, optimization of the size of the WSR is undertaken in Subroutine-3 (Fig. 9) for each configuration s .

To minimize the size of the reservoir in Subroutine-3, the system is forced to be operational throughout the year (Fig. 8). Prior to executing Subroutine-3, the maximum volume of water, $MV_0^s = \max(V_{o,i}^s)$ with $i = 1, \dots, ny$, which the reservoir must contain before starting up the system, is determined for each configuration s . Likewise, the reservoir volume, $V_{s,i}^s = V_{s,i}^s + MV_0^s - V_{o,i}^s$, required in each of the i years considered, is determined for each configuration s .

As can be observed in Fig. 9, for the configuration s , the algorithm starts with the reservoir volume, V_s , defined in Subroutine-2, and reduces it by an amount that is equal to the hourly production of an SWRO module whilst meeting the requirement that there is sufficient wind energy potential to power at least one SWRO module, whether or not it is operational, and the requirement that the water volume in the reservoir at the end of the year is equal (with a tolerance T) to V_o .

2.3.5. Calculation of the specific cost of the water produced with each configuration s of the system

After the different configurations s of the system which meet the

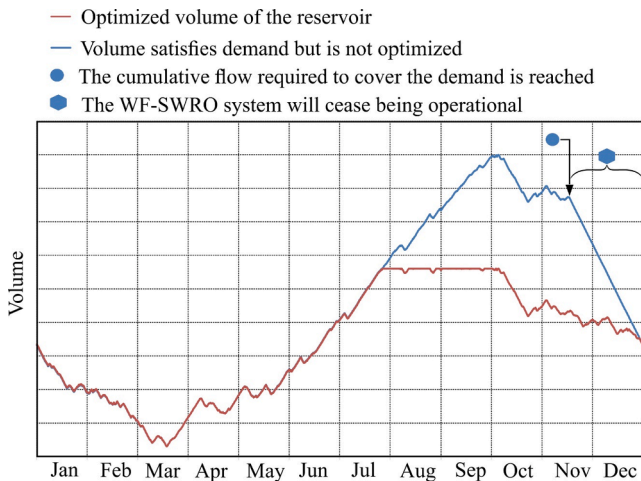


Fig. 8. Optimization of water storage reservoir.

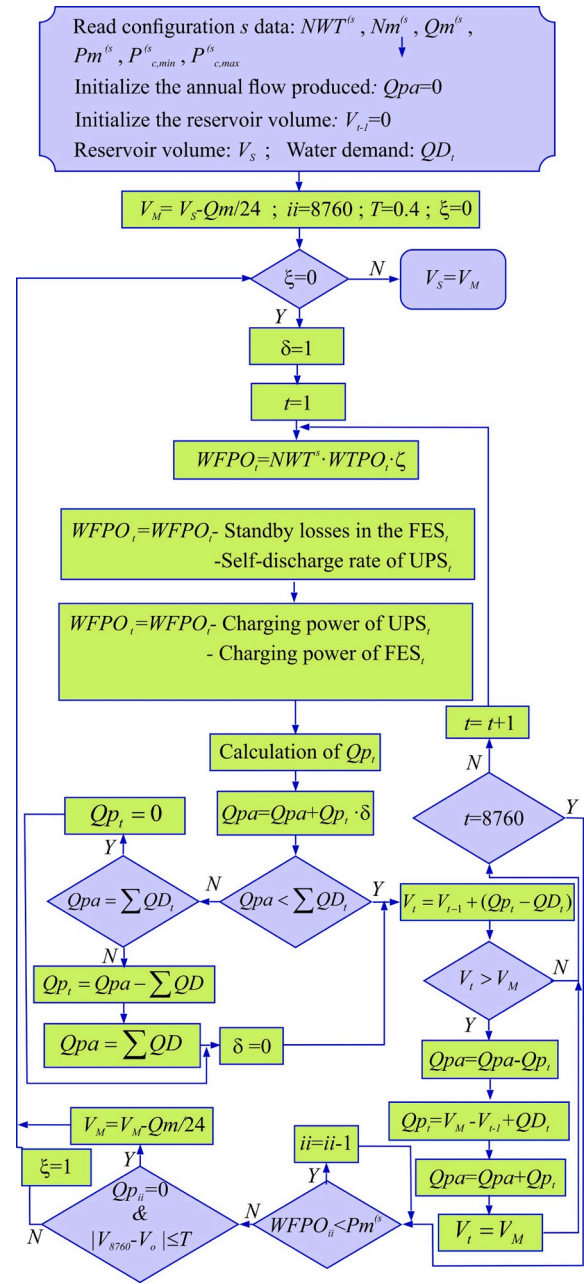


Fig. 9. Subroutine-3. Estimation of the minimum volume of the reservoir, V_s , for each year and configuration s .

requirement of covering annual freshwater demand have been fully defined, and after the sizes of the WSR have been optimized, Subroutine-4 undertakes the analysis of the specific cost per m^3 of product water in each of the configurations. To select the optimal configuration from an economic perspective, use is proposed in this study of the so-called simplified cost of water (SCOW) method [58], Eq. (13), which has been extensively used in the literature.

$$SCOW = \frac{TPV \cdot CRF + \text{Annual O\&M costs}}{\sum_{t=1}^{8760} QD_t}, \text{ in } \text{€}/\text{m}^3 \quad (13)$$

In Eq. (13), TPV is the total present value of the actual cost of all the subsystems of a given configuration s . That is, TPV , Eq. (14), takes into account the costs associated with the investments that need to be made in the electrical energy generation subsystem (C_{WF}), the dynamic regulation subsystem (C_{FES}), the energy storage subsystem ($C_{Batt}^{I\&R}$), the water desalination subsystem (C_{SWRO}) and the water storage reservoir

subsystem (C_{WSR}). Annual O&M costs correspond to the costs associated with the operation and maintenance of the system, Eq. (15).

$$TPV = C_{SWRO} + C_{WSR} + C_{WF} + \psi \cdot C_{FES} + C_{Batt}^{I\&R} \quad (14)$$

$$Annual\ O\&M\ costs = C_{SWRO}^{O\&M} + C_{WSR}^{O\&M} + C_{WF}^{O\&M} + \psi \cdot C_{FES}^{O\&M} + C_{Batt}^{O\&M} \quad (15)$$

In the cases in which massive energy storage is discarded, $C_{Batt}^{I\&R}$ represents the initial investment costs, C_{Batt} , and the replacement costs, C_{Bat}^R , Eq. (16), of the UPS. In the RS case, these costs refer to the battery-based massive energy storage subsystem. $\psi = 1$ if massive energy storage devices are not used, otherwise $\psi = 0$.

$$C_{Batt}^{I\&R} = C_{Batt} + C_{Bat}^R = C_{Batt} + C_{Batt} \cdot \underbrace{\left[\frac{1}{(1+i)^{y_1}} + \frac{1}{(1+i)^{y_2}} + \dots \right]}_{C_{Bat}^R} \quad (16)$$

In Eq. (16), C_{Bat}^R depends, as indicated by van den Boomen *et al.* [59] and Díaz-González *et al.* [60], on the periods, y_1, y_2, \dots , in which the battery replacements are performed and on the discount rate, i , that is used, which represents to a certain degree the opportunity cost of the resources employed.

The CRF, Eq. (17), is the capital recovery factor, which is dependent on the useful life, L , of the system and the discount rate, i .

$$CRF = \frac{i \cdot (1+i)^L}{(1+i)^L - 1} \quad (17)$$

2.4. Task-4. Modelling of the reference system. Comparison with the reference case

In the case of the RS, it is firstly necessary to establish the capacity, $Nm \times Qm$, of the SWRO plant that can cover the annual water demand, $\sum_{t=1}^{8760} QD_t$. Likewise, it is necessary to determine the volume of the WSR that balances the mismatches between the product flow, Qp_b , of the SWRO plant and the water demand, QD_b , at each instant t . This volume is estimated in a similar way to that indicated in Subroutine-2 (Fig. 7). The WF must have an NWT that allows the generation of the power required by the SWRO to meet the annual water demand, $\sum_{t=1}^{8760} QD_t$. The batteries must be able to store the energy that is necessary to balance the mismatches between the power output of the WF, $WFPO_t$ and the power, $P_c = Nm \times Pm$, consumed by the SWRO plant at each instant t . For each instant t , the battery charging and discharging processes are undertaken using the mathematical models indicated in Eqs. (18) and (19), respectively:

$$E_{Batt,t} = E_{Batt,t-1} \cdot (1 - \sigma_t) + (WFPO_t - P_c) \cdot \sqrt{RTE}; WFPO_t > P_c \quad (18)$$

$$E_{Batt,t} = E_{Batt,t-1} \cdot (1 - \sigma_t) - (P_c - WFPO_t) / \sqrt{RTE}; WFPO_t < P_c \quad (19)$$

where RTE is the round-trip DC-to-storage-to-DC energy efficiency of the batteries and the electronic power converters and σ_t is the set discharge rate in the time t [12]. In this model, it was considered that there exists an annual RTE degradation percentage, $RTEDA$. The charging and discharging of the batteries are undertaken in such a way that in the control of their state of charge (SOC) at an instant t , defined through Eq. (20), the maximum depth of discharge (DOD) is limited [12].

$$(100 - DOD) \leq SOC_t = \frac{E_{Batt,t}}{NBC} \cdot 100 \leq 100 \quad (20)$$

where NBC is the nominal battery capacity.

2.5. Task-5. Simulation of the optimal system

In this task, the simulation was undertaken of the system that was determined to be optimal in Task-3. Knowing the optimal configuration (NWT, Nm , V_s), and using a loop that covers all the hours of the years

analysed, the wind power available in the WF in each hour is determined, along with the number of SWRO modules in operation, the flow produced, the values of the operating parameters of each SWRO module (power consumed, operating pressure and recovery rate), the available power of the WF not used by the desalination system, and the available volume of water in the WSR. For more detailed information, please consult the Supplementary Material (S.4: Task-5).

3. Case study

In this section, the location of the system is described and the wind and freshwater demand data are presented. Information is also given about the costs of the WSRs, as well as technical and economic data about the WTs, batteries, FES and the SWRO modules.

3.1. Location of the system in the case study

The case study of the proposed method was undertaken on the island of Gran Canaria (Canary Islands-Spain). Fig. 10 shows the location of WS-4 where the wind data of the installation site proposed for the system were recorded. The locations of WS-1, WS-2 and WS-3 are also shown, where the historical long-term mean hourly wind data series were registered and which will be considered the reference stations when MCP methods based on RF [44] are used to estimate the wind speeds at the target site, WS-4, for which only short-term wind data series are available.

3.2. Description of the meteorological data used

For the purpose of this study, we used the mean hourly wind speed and directions recorded at a height of 10 m above ground level (a.g.l.) during the period 2001–2019 at the reference stations (WS-1, WS-2 and WS-3) installed at the airports of three of the islands in the Canary Archipelago (Fig. 10), and the available mean annual wind speeds (2010 and 2014) recorded at WS-4 (Fig. 10) at a height of 60 m a.g.l.

Fig. 11 shows the interannual variations of the mean wind speeds at the various WSRs.

Fig. 12 shows a boxplot of the mean monthly wind speeds recorded at the three reference WSRs, revealing the seasonal variability of the wind and its greater intensity during the summer months due to the influence of the trade winds.

For more detailed information, please consult the Supplementary Material (S.5: Meteorological data used).

3.3. Description of the freshwater demand data used

Fig. 13 shows a boxplot of the mean hourly profile of the variation in freshwater demand used for the purposes of the case study.

The annual flow is 1,825,000 m³/year, which is equivalent to the water production of a desalination plant with a 5000 m³/day capacity operating continuously 365 days of the year. Fig. 14 shows the monthly freshwater demand which the proposed wind energy powered desalination system aims to cover. For more detailed information, please consult the Supplementary Material (S.6: Freshwater demand data used).

3.4. Description of wind turbine technical and economic data

For this study, we opted to use E-44 and E-70 WTs manufactured by Enercon GmbH. For this reason, the bounds of the variable WTT are {1,2}. The WTs have respective rated powers of $P_r = 900$ kW and $P_r = 2300$ kW [61] and are widely used in WFs in the Canary Islands. In this case study, a hub height of 60 m was considered.

In order to estimate the investment costs of the WFs, an analysis was undertaken of the costs of 10 WFs made up of E-44 WTs and 11 WFs made up of E-70 WTs, recently installed in the Canary Islands (Table 1).

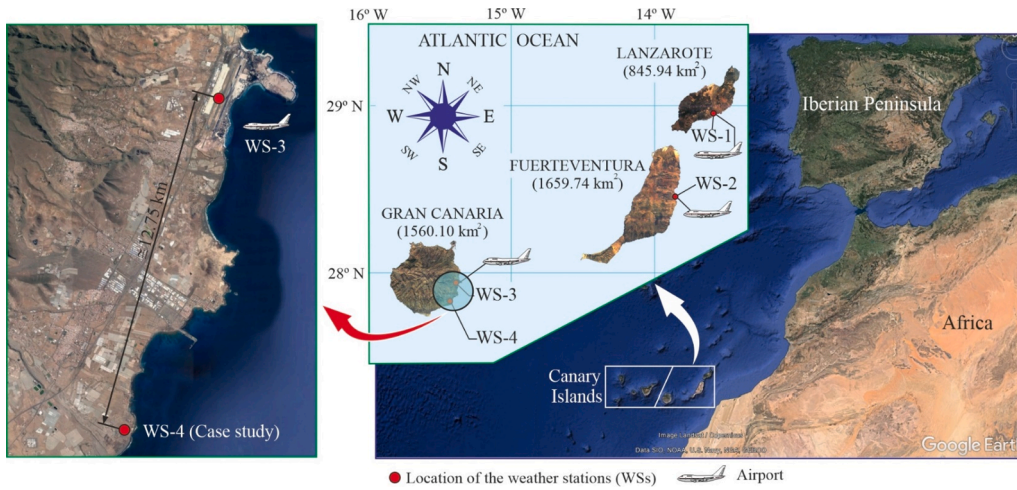


Fig. 10. Location of the case study.

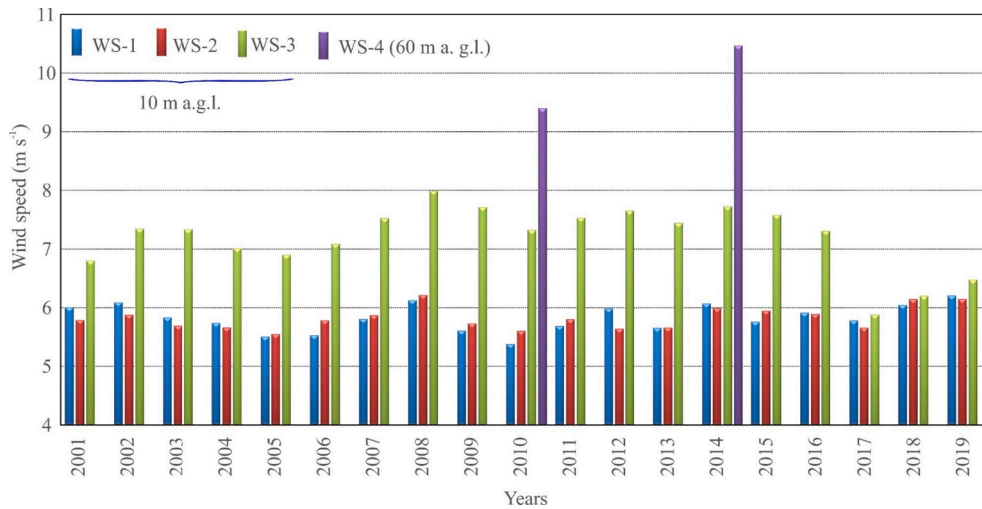


Fig. 11. Mean annual wind speeds recorded during the 2001–2019 period at the reference stations (WS-1, WS-2 and WS-3) and the available mean annual wind speeds (2010 and 2014) recorded at the target site (WS-4) at respective heights of 10 m and 60 m a.g.l.

In this work, the total investment costs (€) in the WF are given by Eqs. (21) and (22) for the case of the E-44 and the E-70, respectively.

$$C_{WF}(NWT) = (1.1481 \cdot NWT - 0.5308) \cdot 10^6 \quad (21)$$

$$C_{WF}(NWT) = (2.19 \cdot NWT - 0.05) \cdot 10^6 \quad (22)$$

For more detailed information, please consult the Supplementary Material (S.7: Wind turbine - technical and economic data).

The annual operating and maintenance cost, $C_{WF}^{O\&M}$, of the generation system was taken as $\eta = 3.3\%$ of the investment cost [83], Eq. (23):

$$C_{WF}^{O\&M} = \eta \cdot C_{WF} \quad (23)$$

3.5. Description of SWRO module technical and economic data

The capacities of the modules considered in this work (Table 2) and their nominal operating characteristics were obtained using the Toray software [57]. The bounds of the variable MT are $\{1,9\}$. For more detailed information, please consult the Supplementary Material (S.8: SWRO module technical data).

The maximum and minimum operating powers of each SWRO module are given in Table 2.

The specific costs, $c_{SWRO}(Qm)$, in $\text{€}/\text{m}^3$, associated to the different

desalination capacities are given through Eq. (24) [29].

$$c_{SWRO}(Qm) = 4151.8 \cdot Qm^{-0.125} \quad (24)$$

Estimation of the total investment cost of a given configuration, s , of an SWRO plant comprising Nm^s modules was made through Eq. (25) [29]:

$$C_{SWRO} = \alpha \cdot c_{SWRO}(Qm) \cdot Nm^s \cdot Qm + (1 - \alpha) \cdot c_{SWRO}(Qm \cdot Nm^s) \cdot Nm^s \cdot Qm \quad (25)$$

In Eq. (25), $\alpha = 0.75$ [29] reflects the percentage of specific investment costs attributable to the cost of mechanical equipment, membranes, electrical and instrumentation systems and ERDs. The remaining $(1-\alpha)$ of the investment costs includes intake construction costs, intake pump stations, building costs, brine and product flow discharge and indirect capital costs [84].

The annual operating and maintenance costs are expressed in this work by Eq. (26). The value of $0.106 \text{ €}/\text{m}^3$ for product water is the sum of the cost attributable to the use of chemicals ($0.044 \text{ €}/\text{m}^3$ [85]) and the cost ($0.062 \text{ €}/\text{m}^3$ [85]) attributable to membrane and cartridge filter replacement. The second term of Eq. (26) represents the fixed operating and maintenance costs and was estimated as a percentage ($\beta = 4\%$ [85]) of the investment costs.

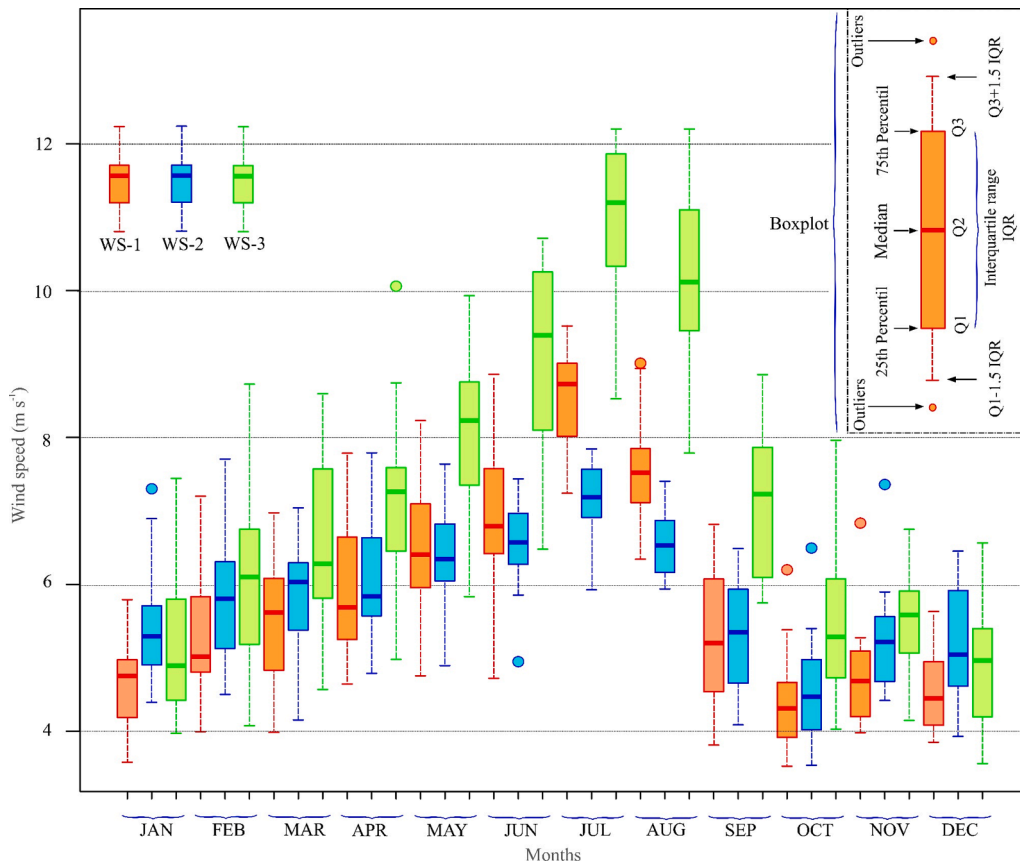


Fig. 12. Boxplot of the mean monthly wind speeds recorded at the reference stations WS-1, WS-2 and WS-3 during the 19 years considered (2001–2019).

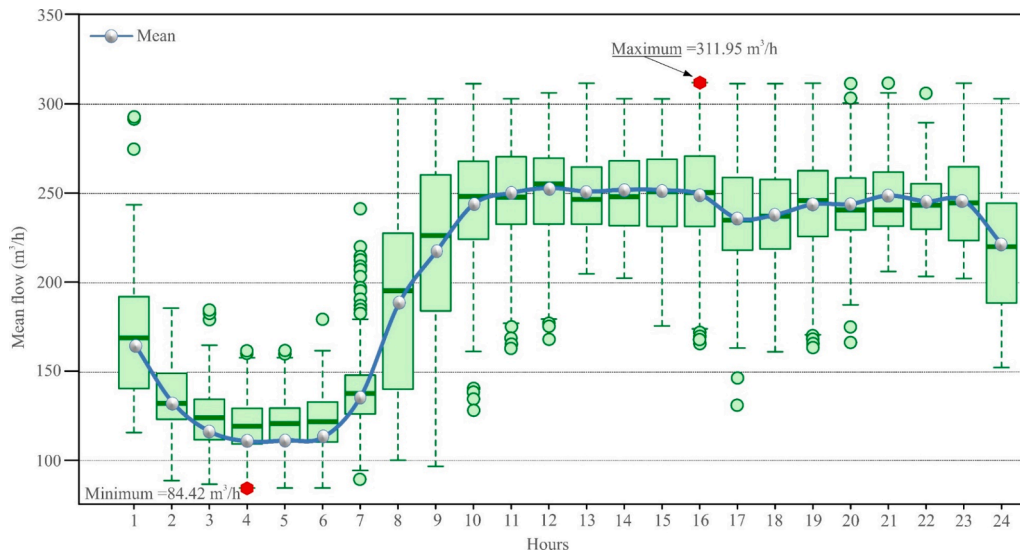


Fig. 13. Daily flow profile, constructed using one year of mean hourly flow data.

$$C_{SWRO}^{O\&M} = 0.106 * \sum_{t=1}^{8760} Qp_t + \beta * C_{SWRO} \quad (26)$$

3.6. Description of WSR costs

Eq. (27) shows the specific investment cost, $c_{WSR}(V_s)$, in concrete, covered-type WSRs according to their capacity. This cost was calculated on the basis of data obtained for different WSRs constructed in Spain

with volumes ranging from 1000 m³ [86] to 60000 m³ [87].

$$C_{WSR}^{O\&M} = C_{WSR} * \gamma \quad (27)$$

For more detailed information, please consult the Supplementary Material (S.9: Specific costs of the water storage).

A logarithmic curve, Eq. (28), was fitted to this data with a coefficient of determination of $R^2 = 0.8646$. The specific cost above 70000 m³ was assumed to remain constant.

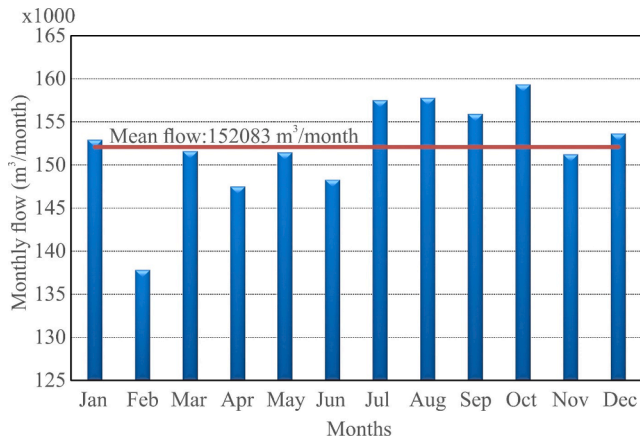


Fig. 14. Monthly average freshwater demand.

$$c_{WSR}(V_s) = -30.55 \cdot \ln(V_s) + 441.73 \quad (28)$$

That is, the investment cost in the water storage system will be given by Eq. (29):

$$C_{WSR} = c_{WSR}(V_s) \cdot V_s \quad (29)$$

The annual operating and maintenance costs are usually estimated as a percentage of the investment cost, and, in this work, this was taken as $\gamma = 0.015$ [88], Eq. (27).

3.7. Description of battery subsystem technical and economic data

The investment cost of the Li-ion battery subsystem is given by Eq. (30) and the specific cost, c_{Batt} , was obtained from [89]. $c_{Batt} = 297$ €/kWh includes the cost of the power conversion subsystem (PCS), the balance of plant (BOP) and construction and commissioning (C&C). Replacement cost was estimated through Eq. (16) and considering a useful life of 10 years. $c_{Batt}^{O\&M}$, Eq. (31), was estimated considering a fixed cost of 6.6 €/kW and a variable cost of 0.025 €/kWh [89]. An RTE = 86% was considered and a charging efficiency equal to that of discharging. The following were also considered: $\sigma_t = 0.02\%$ [90], RTEDA = 0.5%, DOD = 80%, $P_{control} = 0.3$ kW and $P_{swt} = 20$ kW [91].

$$C_{Batt} = c_{Batt} \cdot E_{Batt} \quad (30)$$

$$C_{Batt}^{O\&M} = 6.6 \cdot P_{Batt} + 0.00025 \cdot E_{Batt} \quad (31)$$

3.8. Description of FES technical and economic data

The costs associated to the FES were obtained from [89]. The specific cost considered, which includes the PCS, BOP and C&C costs, was $c_{FES} = 2361$ €/kW, Eq. (32). $c_{FES}^{O\&M}$ was estimated considering a fixed cost of 4.6 €/kW and a variable cost of 0.025 €/kWh [89]. The following were also considered: $w_{min} = 5760$ rpm, $w_{max} = 6240$ rpm, $\phi = 50\%$, and a useful

Table 1
Number of WTs in WFs and references.

E-44	1 [62]	1 [63]	1 [64]	21 [65]	2 [66]	2 [67]	10 [68]	7 [69]	9 [70]	2 [71]	
E-70	1 [72]	1 [73]	1 [74]	3 [75]	4 [76]	4 [77]	6 [78]	7 [79]	8 [80]	3 [81]	4 [82]

Table 2
Ranges of power consumption, P_c , of the SWRO modules considered.

MT	1	2	3	4	5	6	7	8	9
Q_m (m ³ /day)	1000	1500	2000	2500	3000	3500	4000	4500	5000
P_{min} (kW)	87.11	130.67	174.22	217.78	261.33	202.01	348.47	392.03	435.58
P_{max} (kW)	144.24	216.35	286.16	360.56	432.67	377.44	576.88	649.02	721.12

life greater than 25 years.

$$C_{FES} = c_{FES} \cdot P_{FES} \quad (32)$$

$$C_{FES}^{O\&M} = 4.6 \cdot P_{FES} + 0.00025 \cdot E_{FES}$$

4. Results and discussion

The results obtained in the different tasks indicated in Fig. 2 are presented and analysed in this section.

4.1. Task-1. Analysis of the results obtained in the estimation of long-term wind speed

From the analyses undertaken in Task-1 (Fig. 2) with M-1 (Eq. (1)) of the estimation of long-term wind speed at the target site, it is deduced that none of the input features initially considered were discarded by the wrapper method. The RFE algorithm [51] indicates that the best subset size was estimated to be 9 predictors, namely the 9 input variables initially considered, Eq. (1). That is, all the variables used as M-1 model inputs (wind speeds and directions of the three reference WSs) contributed in reducing the forecasting error of the variable wind speed at the target site, which is the output variable of the model. This result is in agreement with the results obtained in previously published works [92] in which the improvement in wind speed forecasting was demonstrated when using various reference WSs as opposed to using MCP models based on the use of just a single reference WS.

It is therefore recommended, when estimating the long-term wind speed at a site under consideration for the installation of systems analysed in the present study, to use MCP models that can incorporate regional information of the wind resource and that use a wrapper method.

The R_a^2 mean value of 81.33% (with a standard deviation of 1.07%) and the IoA mean value of 0.8151 (with a standard deviation of 0.001) reflect a relatively good goodness-of-fit of the M-1 model to the variable wind speed at 60 m a.g.l. at the target site. The MAE value of 1.521 ms⁻¹ (with a standard deviation of 0.047 ms⁻¹) indicates the mean absolute error of the target variable that it is estimated will be produced if the hypothesis of climate stability on which the MCP methods are based is met [33]. It should be noted that, probably, if the variables recorded at 10 m a.g.l. at the reference WSs had been used to estimate the wind speeds at 10 m a.g.l. at the target WS, the forecasting errors would have been lower. However, in this situation, to evaluate the wind speeds at 60 m a.g.l. based on the estimated wind speeds at 10 m a.g.l. at the target WS, a vertical wind profile model would be required in which terrain roughness length would have to be considered [53] as a function of wind direction, as well as atmospheric stability (neutral, unstable, stable) [53]. For this, it would be necessary to estimate not only the long-term wind speeds but also the long-term wind directions. This, coupled with the uncertainty that the vertical wind profile model generates, can lead to errors higher than those obtained with the procedure used in the present paper.

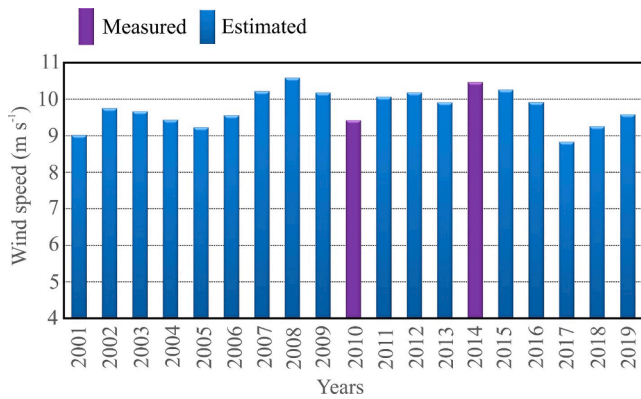


Fig. 15. Mean measured and estimated annual wind speeds at 60 m a.g.l. with M-1 during the 2011–2019 period at the target station WS-4.

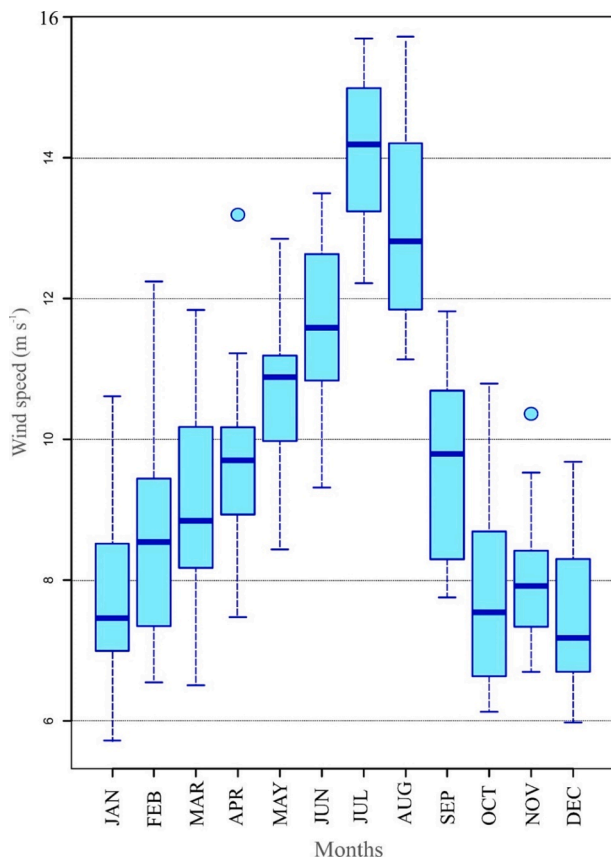


Fig. 16. Boxplot of the mean monthly estimated wind speeds at 60 m a.g.l. at WS-4 with M-1 for the study period (2001–2019).

Fig. 15 shows the interannual variations in mean estimated wind speeds at 60 m a.g.l. with M-1, and Fig. 16 a boxplot of the mean monthly estimated wind speeds at 60 m a.g.l. in WS-4.

It can be seen that the mean annual wind speeds can differ by more than 1 m/s and that, although a certain trend is maintained in seasonal wind behaviour, the interannual variation of the mean wind speed in a given month can present significant differences and atypical values (outliers). The above analysis justifies the need to consider the inter-annual and seasonal evolution of wind speed when evaluating the proposed desalination system, as opposed to the use of deterministic models or models which use only one series of annual wind speed data as has been the case to date in the scientific literature [30].

For more detailed information, please consult the Supplementary

Material (S.10: Results obtained in the estimation of long-term wind speed).

4.2. Task-2. Analysis of the influence on the results of the randomization of the daily profile of freshwater demand

As indicated in Section 2.2, in the proposed method the randomness of the daily water demand profile was considered. Evidently, the randomness of this demand together with the randomness of the mean hourly wind speeds have a considerable influence on the output variables of the simulation model used, including the operating frequencies of the SWRO modules, the water volumes in the WSR, the percentages of unused available wind energy, etc. However, in this work, the contribution of the inherent uncertainty due to the random nature of each of these two input variables of the estimation model to the uncertainty of the response of the model was not quantified. This corresponds to a knowledge gap that we propose to resolve in future works using a global sensitivity analysis model. In this context, use is proposed of the method employed by Carta *et al.* [93] for WF power output estimation models, which can be applied both if there is dependency between the input variables and if they are independent.

4.3. Analysis of the results obtained in the system optimization

In this work, L was estimated at 20 years and i at 5% of investments at constant prices, Eq. (17). Table 3 shows the configurations that were optimal for each WTT and SWRO plant operating strategy.

It can be deduced that, for a given operating strategy, the WFs comprised of WTs with higher rated power ($WTT = 2$) give a lower specific product water cost. This justifies our proposal for the use, whenever possible, of higher rated power WTs for these applications. That is, economy of scale has an influence on the product water cost. This question was also highlighted in a study by Kyriakarakos and Papadakis [15] on small-scale desalination coupled with renewable energy. In fact, there has been a rising trend, fundamentally in Europe, of the rated power of WTs installed over recent years [94]. In Europe, in 2019 and according to the data available for 14 countries, the average power rating of new onshore WTs was 3.1 MW [95]. Nonetheless, in places like the Canary Islands, where the case study was developed, $WTT = 1$ continue to be installed (Table 1).

It can be observed that the S-2 strategy provided, in all the analysed configurations in the case study, lower specific costs than the S-1 strategy. The S-2 strategy allows the SWRO modules to take more efficient advantage of the wind energy, enabling a reduction in their number while maintaining or even reducing the number of WTs (Table 3).

It can be seen that, although the capacities of the SWRO modules considered are in the range of 1000–5000 m³/day (Table 2), the algorithm of the optimization preferentially selected the capacities of the smaller modules (1000 and 1500 m³/day). This is a consequence of the fact that these capacities, despite requiring a higher Nm than with the higher capacity modules, are more suitable in terms of adapting the consumption of the SWRO plant to the hourly wind energy variation and generating a lower specific product water cost. The lowest specific cost (2.08 €/m³) was obtained with the configuration of $WTT = 2$, $Nm = 8$, $NWT = 5$ and $Qm = 1000$ m³/day. The variability of the wind and the absence of massive energy storage systems require the optimal system obtained to have a desalination plant with a global capacity of 8000 m³/day, which is considerably higher than the 5000 m³/day which would be required to cover the annual freshwater demand if the plant were to operate conventionally, as is the case of the RS. However, it is deduced from the results obtained with the S-1 and S-2 operating strategies (using modules of 1000 m³/day) that, despite requiring respective installed capacities of 9000 m³/day and 8000 m³/day, these strategies result in lower product water costs than the RS systems (Table 3).

This specific cost is within the 0.56€/m³–3.15€/m³ range generated,

Table 3
Optimal configurations.

Strategy	WTT	NWT	Nm	Qm m ³ /day	Volume Htm ³	UPS/Bat MWh	FES kW	Investment M€	Cost €/m ³
S-1	1	9	7	1500	0.1046	6.4	678	42.00	2.61
S-2	1	8	6	1500	0.1163	5.7	775	39.21	2.42
S-1	2	5	9	1000	0.0745	1.0	581	35.42	2.25
S-2	2	5	8	1000	0.0659	1.0	323	32.57	2.08
RS	1	18	1	5000	0.0187	102.4	–	78.13	4.45
RS	2	7	1	5000	0.0187	76.5	–	61.09	3.52

according to Karagiannis and Soldatos [96], by SWRO plants with capacities of between 1000 m³/day and 5000 m³/day. It can also be observed that the specific costs of all the configurations that discard the use of massive energy storage were lower than those generated with the RS, with the latter being higher than the results obtained by Roggenburg et al. [6].

This costs comparison, it should be noted, is solely for illustrative purposes as the wind regime data used in the calculation has a considerable influence on these costs. When performing a more precise comparison, these data need to be homogenised. Given the aim of the present study, the costs comparisons undertaken were based on an identical wind regime, which can be classified as high (mean interannual wind speed above 9.7 m/s at 60 m a.g.l., Fig. 15). Given that product water costs with lower intensity winds will be higher, use of the method described in this work is proposed to carry out this estimation.

It should be noted that the specific cost obtained with the RSs (Table 3) did not contemplate, as did the systems which used the S-1 and S-2 strategies, a volume of the WSR as a safety reserve ($\Delta = 14974 \text{ m}^3$, corresponding, in the case study, to two days of maximum hourly demand, Fig. 13). If this safety reserve is also considered, the specific costs of RS ($WTT = 2$) and RS ($WTT = 1$) would rise to 3.60 €/m³ and 4.53 €/m³, respectively.

Fig. 17 shows the percentages of the investment costs associated to the components of the configurations described in Table 3. It can be observed that, independently of the WTT, use of the S-2 instead of the S-1 strategy entailed a reduction in the investment percentages of the SWRO plant and the WF, but an increase in the investment percentage of

the WSR. In the case of the RS, independently of the WTT, the highest investment percentage is associated to the massive energy storage system. In this case, the investment percentages in the SWRO plant and in the WSR are considerably lower than those that appear in the configurations that discard the use of massive energy storage. Therefore, given the large size of the battery systems and the costs currently associated to such systems, it makes sense to use higher desalination capacities than those used with the RS (which operate without interruption), despite

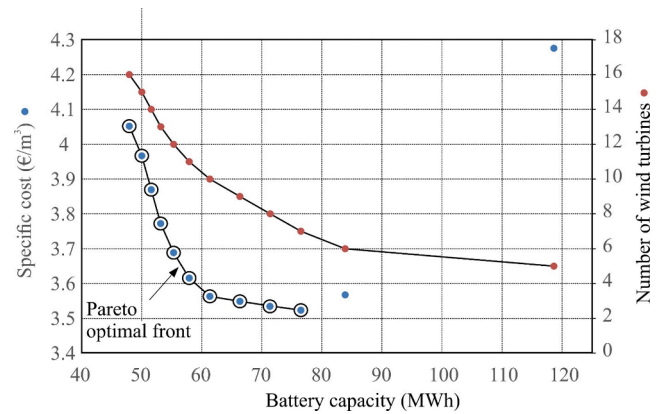


Fig. 18. Specific cost generated by the reference system according to the capacity of the energy storage system and number of wind turbines.

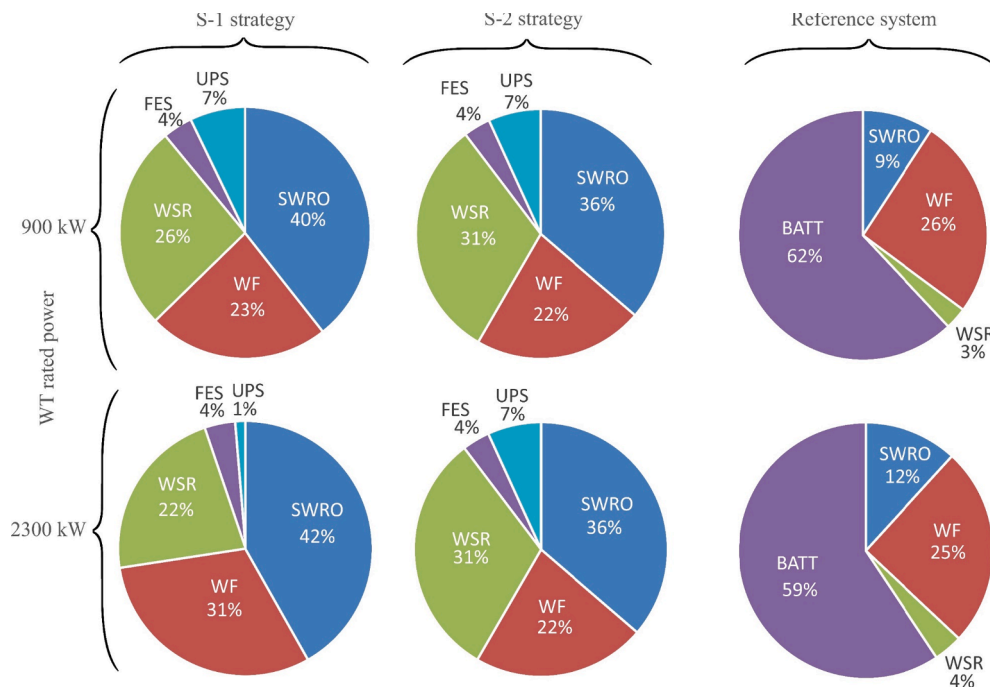


Fig. 17. Specific costs of the product water according to each of the different configurations and operating strategies (S-1 and S-2) of the SWRO modules analysed.

their lower degree of use. A similar conclusion was drawn in [15] in the case of small-scale desalination. In addition, the operating strategies S-1 and S-2, as they discard the use of massive energy storage devices, reduce the high environmental cost that, according to McManus [23], such devices can produce.

In the case of the RS, once the mean daily capacity of the SWRO plant is established (5000 m³/day), the specific product water cost depends fundamentally on the capacities of the WF and the battery systems (Fig. 18). If the aim, in addition to minimizing the specific product water cost, were to also include minimization of battery capacity, it would be necessary to make a decision about the configuration of the system on the basis of the information that the Pareto-optimal front provides (Fig. 18).

The systems which discard the use of massive energy storage in batteries do so by turning to the use, in addition to a non-conventional strategy, of a WSR. In the case study, the optimal economic system gave a lower WSR size than that obtained with the majority of the tested configurations (Fig. 19).

In the case of the existence of constraints as the result, for example, of limitations to subsystem size, limitations to land availability, environmental guidelines, regional policies, etc., other optimal options of the Pareto set or Pareto front could be analysed (Fig. 19). With respect to these limitations, it should be noted that the impacts generated by the construction of WSRs are related to the surrounding area (visual, flora, fauna, etc.) and can be avoided or corrected. Any project that engineers wish to carry out requires an obligatory environmental impact study which is imposed by the relevant authorities, and such a study must include any corresponding corrective measures if they are required.

Fig. 20 shows the results of the analysis of the sensitivity of the specific product water cost of the optimal S-2 configuration to changes in various economic parameters.

It can be seen the investment costs in the SWRO plant, the WF and the WSR have a considerable influence on the specific product water cost.

If the WSR investment costs could be reduced by 42% [97], using an open reservoir instead of a covered reservoir made from concrete, the specific product water cost would fall by 6% with this optimal S-2 configuration (Fig. 20), obtaining a specific cost of 1.96 €/m³. However, in such a circumstance a specific cost of 1.93 €/m³ could be attained with a different configuration (NWT = 4, Nm = 8, Qm = 1000 m³/day, UPS = 805 kWh, FES = 258 kW) that requires a larger WSR (95,007 m³) which is shown encircled in Fig. 21. In this respect, we would like to

point out that in the Canary Islands some of the dams are being redesigned and new water storage reservoirs are being built for use in pumped hydro systems. These new reservoirs do not have to be made of concrete and store water which has been previously desalinated by SWRO plants. We would like to mention that some recently constructed reservoirs, including those that we have designed for use in the hydro-wind plant on the island of El Hierro [98], comprise areas dug out of the ground, compacted and then covered with plastic material.

If a WSR were already available and the only associated costs were for operating and maintenance, the specific product water cost would fall by 14.24%. In this situation, the optimal configuration used in the sensitivity analysis moves to eleventh position (with a specific cost of 1.79 €/m³), behind other configurations highlighted in Fig. 21. The lowest specific cost (1.67 €/m³) was obtained with the abovementioned configuration (indicated in the yellow shaded area of Fig. 21). In this context, it should be noted that the storage of desalinated water in aquifers has been proposed as a possible cost-effective solution for the Gulf Council Cooperation countries [31].

The purpose of the sensitivity or post-optimal analyses was to try to identify the impact on the initial results of certain changes to the variables without having to repeatedly run the algorithm again. Nonetheless, our intention in future works (although at a high computational cost) is to consider and analyse the use of a more appropriate procedure to ensure the robustness of the solution when dealing with variations in the data. This procedure involves including in the optimization method the existing uncertainty in the values of the economic parameters, using for this purpose stochastic optimization or robust optimization [99]. In stochastic optimization [100], the pdfs of the data must be known or estimated. In robust optimization [101], which is more conservative than stochastic optimization, it is considered that uncertain data are included in a so-called uncertainty set which is defined by the user [99].

4.4. Analysis of the results obtained in the simulation of the optimal system

Fig. 22 shows the mean monthly capacity factors (CFs) of the WF for the optimal configuration of the S-2 strategy, as well as the monthly percentages of water produced by the optimal configuration with respect to demand and the mean monthly percentages of WSR occupation. It can be seen that the CFs of the WFs follow, in the case study, the tendency shown by the wind speed at WS-4 (Fig. 19). In the months of July and August, the wind speed at the target site causes the WF to

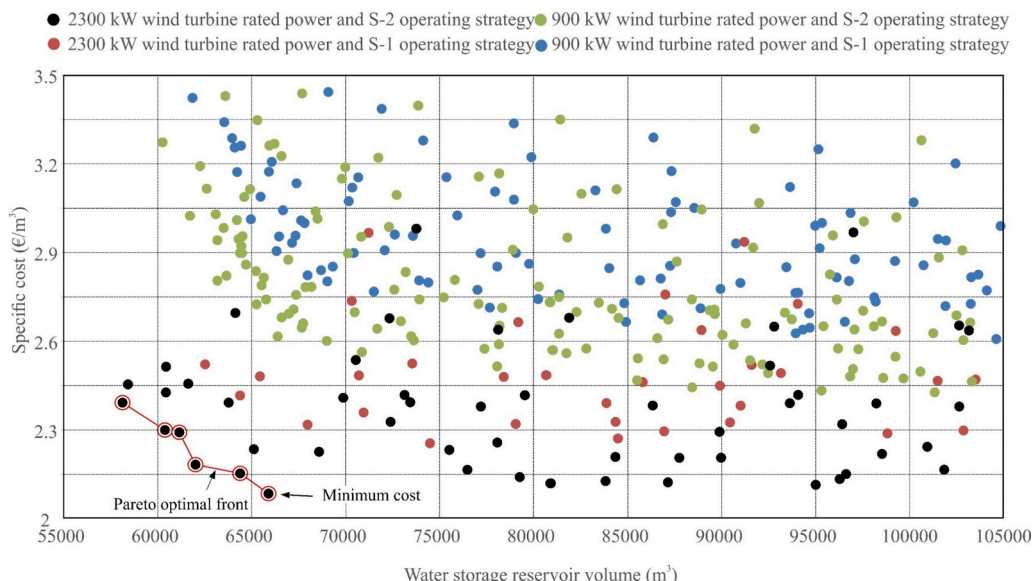


Fig. 19. Specific product water cost according to each of the different configurations and operating strategies (S-1 and S-2) of the SWRO modules analysed.

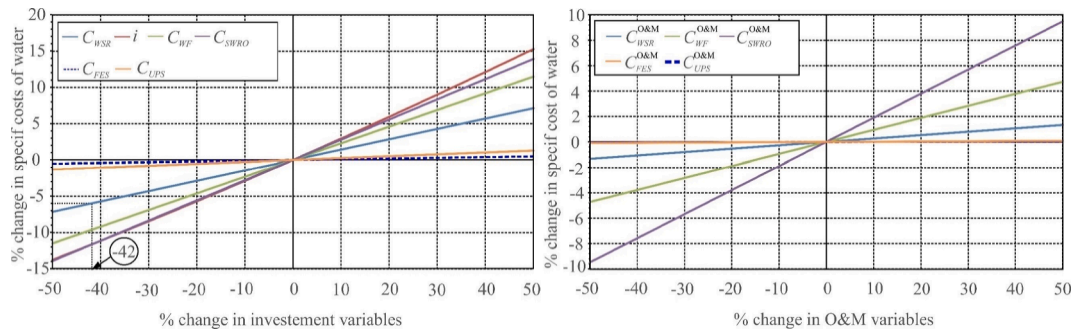


Fig. 20. Analysis of the sensitivity of the specific product water cost of the optimal S-2 configuration to changes in diverse economic parameters.



Fig. 21. Specific product water cost in the case of the need to construct a WSR and in the case of an already available WSR with only operating and maintenance costs to pay.

operate most of the time at its rated power.

Likewise, it can be seen in Fig. 22 that during June, July and August (months with greater influence of the trade winds blowing from the north-east) the WSR is frequently full. Consequently, use of the SWRO modules has to be restricted, despite the availability of wind energy to produce a higher flow of water, due to the WSR size limitation imposed in the system optimization task (Fig. 2) in order to minimize the investment cost and, therefore, the specific product water cost.

It can be seen from the simulation that was performed of the optimal system configuration that the volume of water in the WSR that is not used to cover demand is considerably high (Fig. 23) if compared with that required by the RS (Table 3). It can also be seen that only in 2010 was the water stored in the WSR reduced to the volume established as the safety reserve ($\Delta = 14974 \text{ m}^3$) (Fig. 13). However, in most of the hours (99.05%) of the 19 years considered, the water volume in the WSR was higher than 38995 m^3 . That is, the probability of having a safety reserve greater than 5.2 days, in the worst-case scenario of a 24-hour a day maximum demand of $311.95 \text{ m}^3/\text{h}$ (Fig. 13), is high. This supply guarantee, unlike the RS considered (see Supplementary Material S.11: Simulation of RS), covers contingencies in both the electrical generation system and the water production system, conferring on the supply system a certain capacity of resilience.

Fig. 23 shows the hourly evolution of the volume of water in the WSR over the course of 19 years (2001–2019). It can be seen that, as a

consequence of the interannual variability of the wind regime at the site, the volume of water stored each year can differ significantly. This has an important influence on the size of the WSR that is required to ensure coverage of the hourly water demand with a low degree of uncertainty. In addition, it corroborates the previously mentioned need to discard the possibility of using just one year’s worth of data, despite this being the usual practice in the consulted literature, and take into consideration the interannual variation of wind regimes when estimating the product water costs. In this way, the uncertainty and risks for investors will be reduced.

By way of example, Fig. 23 also shows a simulation of the performance of the UPS and the FES over the course of 2010. It can be seen that the minimum SOC of the UPS was 20%. The mean flywheel operating speeds are also shown for the same year.

The reliability of the water supply in the face of the randomness of the wind and the water demand and in the face of operational contingencies of the WF or SWRO subsystems could be increased by establishing in the optimization method a value of Δ in line with the time period considered convenient. This would evidently entail an increase in the specific product water cost.

It is deduced from the analysis of the data obtained from the simulation of the optimal system configuration that the time during which the SWRO plant was inactive (0 SWRO modules in operation) was lower than the time during which the 8 SWRO modules that make up the plant

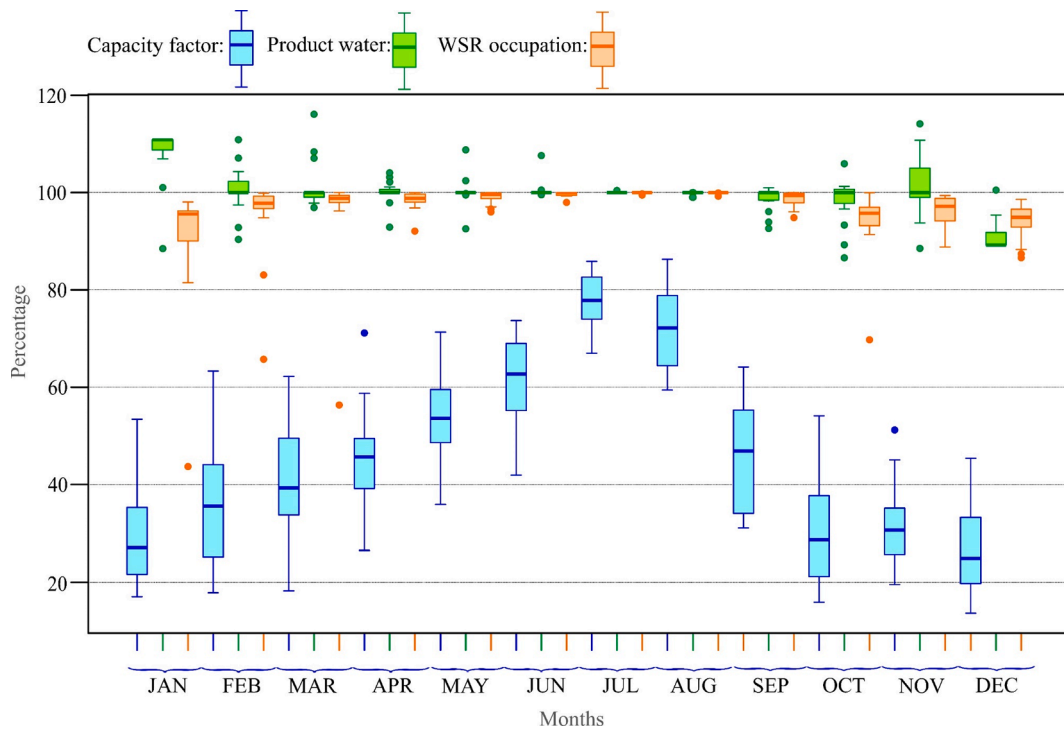


Fig. 22. Mean monthly capacity factors of the WF for the optimal configuration of the S-2 strategy, mean monthly percentages of freshwater produced by this configuration with respect to demand, and mean monthly percentages of WSR occupation.

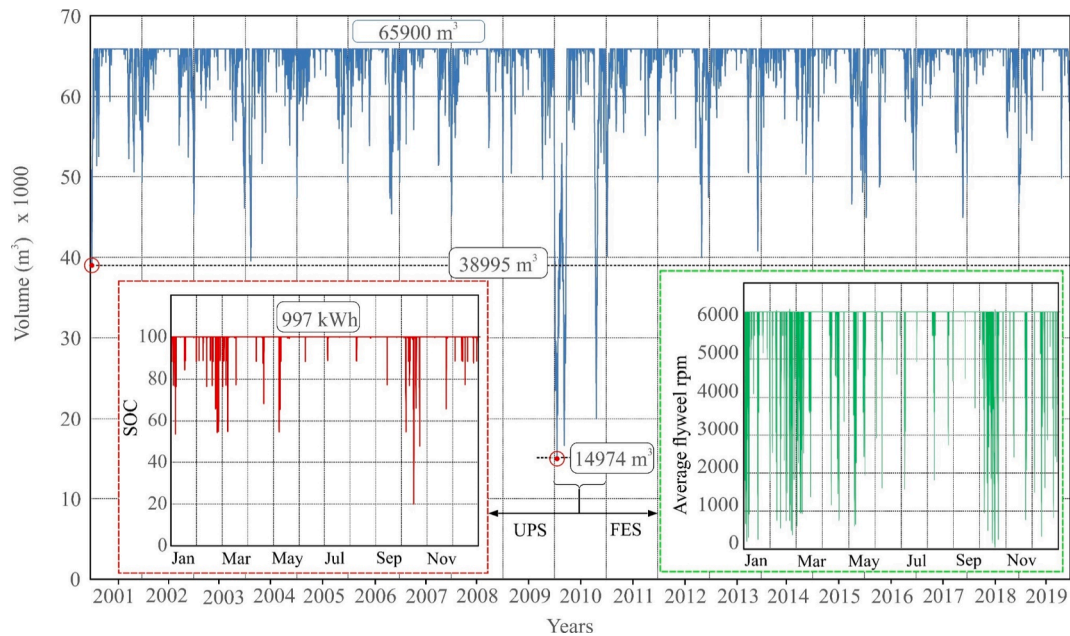


Fig. 23. Hourly volume of water in the WSR for the optimal configuration of the S-2 strategy for each of the 19 years (2001–2019) considered in the study.

were operating simultaneously in parallel (frequency = 15%) (Fig. 24). During 50% of the time, the number of SWRO modules that were operating in parallel was lower or equal to 5 (median of the boxplot of Fig. 24), with the first quartile being 3 SWRO modules and the third quartile 6. That is, during 25% of the time the number of SWRO modules working simultaneously in parallel was less than or equal to 3, and during 75% of the time the number of SWRO modules working simultaneously in parallel was less than or equal to 6.

For more detailed information about the operating ranges of the variables in the optimal configuration of the S-2 strategy, please consult

the Supplementary Material (S.12: Frequencies with which an SWRO module operated for the optimal configuration of strategy S-2).

With the aim of comparing the behaviour of the optimal configuration of strategy S-2 with that of the configurations obtained with strategy S-1, simulations of two configurations were carried out: the optimal S-2 configuration and the S-1 configuration which uses the same SWRO module capacity ($Q_m = 1000 \text{ m}^3/\text{day}$), the same type of WT ($WTT = 2$), the same number of WTs ($NWT = 5$) and the same number of SWRO modules ($Nm = 8$) as the optimal S-2 configuration.

It can be seen (Fig. 25) that the annual number of start-ups/shut-

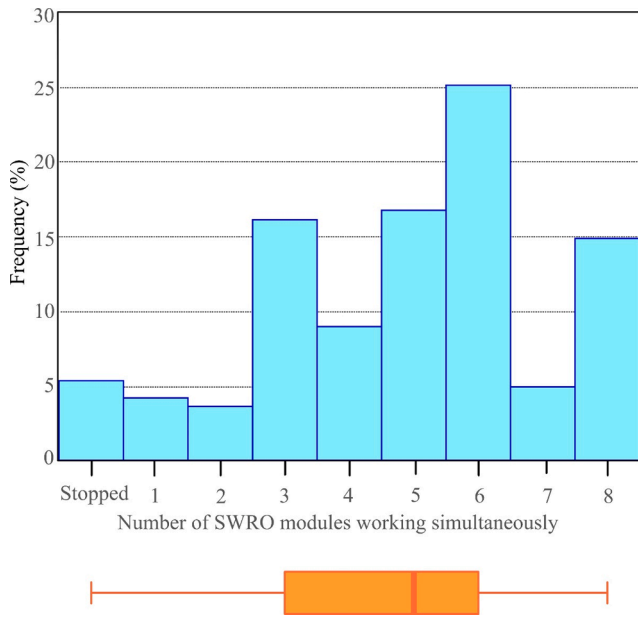


Fig. 24. Frequency (%) of the number of SWRO modules operating simultaneously in parallel in the study period considered.

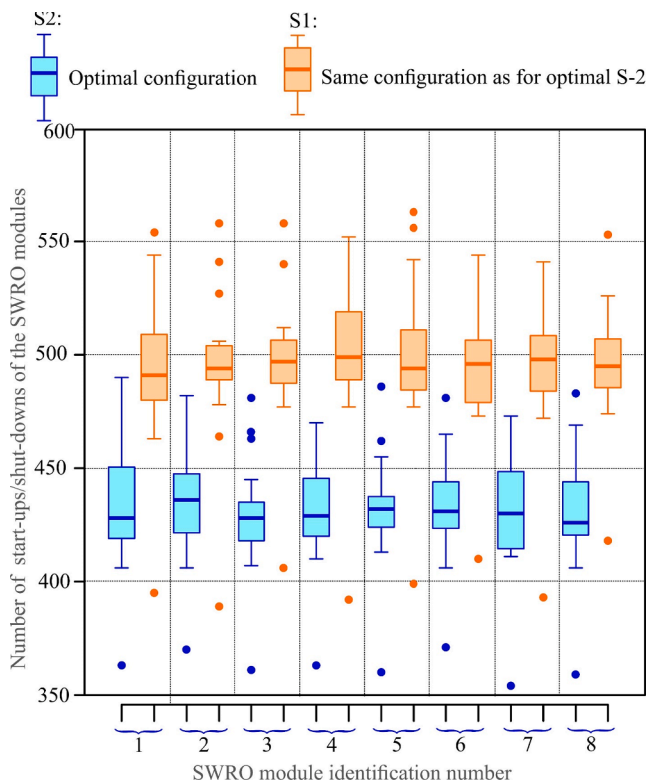


Fig. 25. Comparison of the annual number of start-ups/shut-downs of the SWRO modules generated in the optimal S-2 configuration and the S-1 configuration with the same NWT and Nm as the optimal S-2 configuration.

downs of the modules of the optimal S-2 configuration is lower than that obtained with the S-1 configuration. Given that a quasi-dynamic model was used with time steps of 1 h, the aim with Fig. 25 is not to provide an absolute value of start-ups/shut-downs. The aim is to establish a comparison between the two configurations given that both operate under the same wind speed and water demand conditions. That is, the variable operating strategy allows a reduction in the number of start-ups/shut-

downs of the SWRO modules. Likewise, it can be seen that the optimal S-1 configuration is the one with the highest number of start-ups/shut-downs of the two configurations compared. This is due to the fact that the capacity of these modules operating under constant pressure and flow conditions does not facilitate their adaptation to the variability of the wind energy. In this paper, the so-called ring strategy [27] is applied and as a result, as can be seen in Fig. 25, the disconnection of SWRO modules is undertaken in such a way that the number of start-ups and shut-downs of all the SWRO modules is made approximately uniform.

It should be noted that the S-2 strategy requires a control subsystem that regulates a higher number of parameters than the S-1 strategy. In this context, the implementation of artificial intelligence techniques in wind energy-powered desalination has been proposed [102]. Some results of tests performed in this regard have been published in the scientific literature [38].

With respect to the annual percentages of unexploited wind power, it can be seen in Fig. 26 that the RS configuration is the configuration that best exploits the wind energy that the WF of the system can generate. It can be seen in Fig. 26 that in the S-1 and S-2 optimal configurations the percentage of available but unused wind energy is appreciable.

The load factor of the optimal system, defined as the ratio of the average load divided by the peak load in a specified time period (one year in this case), was calculated as $645.85 \text{ kW}/1153.9 \text{ kW} = 0.56$. The load factor is an indicator of how efficiently energy is being utilized. Given that the load factor is not low, it is seen that energy use is relatively constant.

This energy could be used to optimize system operation by exploiting the unused energy in other applications. In principle, the discarded energy could be used to heat the feedwater of the SWRO modules in order to increase the product water flow. As pointed out by Voutchkov [83], the use of warmer water reduces saline water viscosity, which in turn increases membrane permeability. As a rule of thumb, the permeate flux increases by 3% for every 1 °C of temperature increase. Although

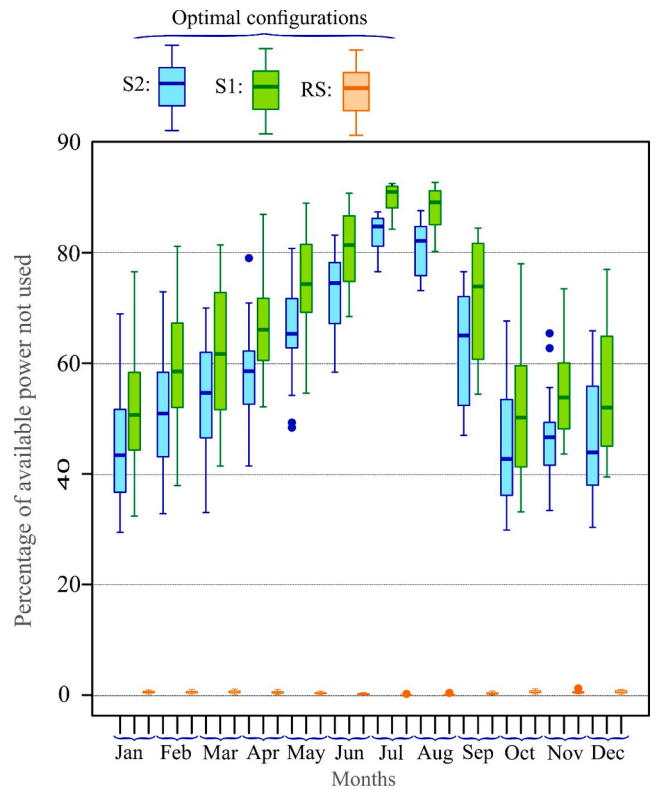


Fig. 26. Monthly percentages of available WF power not used by the SWRO plant. These percentages were analysed for the optimal S-2 configuration, the optimal S-1 configuration, and the RS configuration.

increasing the temperature brings with it an increase in osmotic pressure and can produce an increased passage of salts (lowering the quality of the permeate water) due to the effect of hot water on membrane structure, seawater heated within an acceptable temperature range lowers its viscosity, increasing membrane permeability and thus giving rise to an increase in product water [83]. According to Greenlee *et al.* [103], for source water temperatures up to 30 °C, using warmer water allows reduction of the feed pressure and energy used for desalination.

There also exists the possibility of storing this unused wind energy in the form of H₂ for its use in services unrelated to the system. So-called green H₂, as an energy vector, can be produced through a chemical process known as electrolysis with the use of electrolyzers. This method uses an electrical current to separate the H₂ from the O₂ in water (H₂O). If this electricity is obtained from renewable sources energy will therefore be produced without emitting carbon dioxide into the atmosphere. Likewise, renewable H₂ can be used to generate electricity through the use of hydrogen fuel cells and cover periods of insufficient wind speed. However, there are some doubts about the feasibility of green hydrogen due to its high production cost. According to a report by the International Renewable Energy Agency (IRENA) published in December 2020 [104], strategies to reduce electrolyser costs include continuous innovation, performance improvements and upscaling.

A third alternative to optimize the exploitation of the available wind energy is related to so-called smart demand management [105]. Management strategies can be aimed at adapting, as far as is possible, the profile of water consumption to that of wind energy availability.

With the goal of fighting climate change, strategies are being proposed to achieve substantial reductions in the emission of pollutants into the atmosphere [106]. One of the sectors that can facilitate the transition towards a low carbon emission economy is the energy generation sector. This will entail, amongst other measures, the replacement of fossil fuels with non-polluting renewable energy sources. In this context, the potential contribution of the system proposed in the present study to this transition makes it even more attractive.

5. Conclusions

In this work, a method has been proposed to optimize the design of a system comprising a medium-scale modular seawater reverse osmosis plant -powered exclusively by off-grid wind energy- and a water storage reservoir that allow coverage of a particular freshwater demand without the use of massive energy storage devices. The application of the method to a cases study on the island of Gran Canaria (Spain) has also been analysed.

The proposed method considers the interannual variation of wind energy and for this purpose uses measure-correlate-predict models based on machine learning techniques and introduces randomness in the daily freshwater demand profile.

Of the different results obtained from this study, the following can be highlighted:

- Consideration of the random nature of wind energy and the daily freshwater demand profile gives the method a degree of robustness in its finding viable configurations.
- It is deduced that, for a given operating strategy, wind farms comprising wind turbines with a higher rated power result in a lower specific product water cost.
- A better performance was also observed of the configurations of the modular desalination plants operating under variable conditions compared to their operation under constant conditions. This improvement was detected in the specific product water cost, in the relative frequency of start-ups/shut-downs, and in the better exploitation of the available wind energy.
- The specific costs of all the configurations that discard the use of massive energy storage were lower than those generated with the reference system that does use massive energy storage.

- The proposed system, unlike the reference system that does use massive energy storage, covers contingencies in both the electrical generation system and the water production system, conferring on the supply system a certain capacity of resilience.
- The contribution that the proposed system can make to the transition towards a low carbon emission economy makes it even more attractive.

In summary and in conclusion, the proposed method, which is based on desalination systems powered by wind energy and whose technical operating viability has been previously experimentally demonstrated, constitutes a useful tool for guidance in the design and implementation of such systems.

Declaration of Competing Interest

The authors declare that they have no known competing financial interests or personal relationships that could have appeared to influence the work reported in this paper.

Acknowledgements

This research has been co-funded by the ERDF, the INTERREG MAC 2014-2020 program, E5DES Project (MAC2/1.1a/309). No funding sources had any influence on study design, collection, analysis, or interpretation of data, manuscript preparation, or the decision to submit for publication.

Appendix A. Supplementary material

Supplementary data to this article can be found online at <https://doi.org/10.1016/j.apenergy.2021.117888>.

References

- [1] Kucera J. Introduction to desalination. In: Kucera J, editor. *Desalination. Water from water*. 2nd ed. New York: Wiley; 2019. p. 1–49.
- [2] Khaled Elsaid, Enas Taha Sayed, Bashria A.A. Yousef, Malek Kamal Hussien Rabaia, Mohammad Ali Abdelkareem, A.G. Olabi. Recent progress on the utilization of waste heat for desalination: A review. *Energy Convers Manage* 2020;221:113105. <https://doi.org/10.1016/j.enconman.2020.113105>.
- [3] Gómez-Gotor A, Del Río-Gamero B, Prieto I, Casañas A. The history of desalination in the Canary Islands. *Desalination* 2018;428:86–107.
- [4] Dai J, Wu S, Han G, Weinberg J, Xie X, Wua X, et al. Water-energy nexus: A review of methods and tools for macro-assessment. *Appl Energy* 2018;2210: 393–408.
- [5] Padrón I, Avila D, Marichal GN, Rodríguez JA. Assessment of Hybrid Renewable Energy Systems to supplied energy to Autonomous Desalination Systems in two islands of the Canary Archipelago. *Renew Sustain Energy Rev* 2019;101:221–30.
- [6] Roggenburg M, Warsinger DM, Bocanegra-Evans H, Castillo L. Combatting water scarcity and economic distress along the US-Mexico border using renewable powered desalination. *Appl Energy* 2021;291:116765.
- [7] Ghaffour N, Lattemann S, Missimer T, Choon K, Sinha S, Amy G. Renewable energy-driven innovative energy-efficient desalination technologies. *Appl Energy* 2014;136:1155–65.
- [8] González J, Cabrera P, Carta JA. Wind energy powered desalination systems. In: Kucera J, editor. *Desalination. Water from Water*. 2nd ed. New York: Wiley; 2019. p. 567–646.
- [9] Segurado R, Madeira JFA, Costa M, Duic N, Carvalho MG. Optimization of a wind powered desalination and pumped hydro storage system. *Appl Energy* 2016;177: 487–99.
- [10] Kondili E. Special Wind Power Applications. In: Sayigh A, editor-in-chief, Kaldellis JK. volume editor. *Comprehensive Renewable Energy*, vol. 2. Elsevier; 2012, p. 726–46.
- [11] Carta JA, González J, Gómez C. Operating results of a wind-diesel system which supplies the energy needs of an isolated village community in the Canary Islands. *Sol Energy* 2003;74:53–63.
- [12] Mokheimer EMA, Sahin AZ, Al-Sharafi A, Ali AI. Modeling and optimization of hybrid wind-solar-powered reverse osmosis water desalination system in Saudi Arabia. *Energy Convers Manage* 2013;75:86–97.
- [13] Guzmán-Acuña L, Lake M, Vasquez-Padilla R, Lim LY, González-Ponzón E, Too ICS. Modelling autonomous hybrid photovoltaic-wind energy systems under a new reliability approach. *Energy Convers Manage* 2018;172:356–69.

- [14] Ibrahim MM, Mostafa NH, Osman AH, Hesham A. Performance analysis of a stand-alone hybrid energy system for desalination unit in Egypt. *Energy Convers Manage* 2020;215:112941.
- [15] Kyriakarakos G, Papadakis G. Is small scale desalination coupled with renewable energy a cost-effective solution? *Applied Sciences*. 2021;11(12):5419. <https://doi.org/10.3390/app11125419>.
- [16] Elmaadawy K, Kotb KM, Elkadeem MR, Sharshir SW, Dán A, Moawad A, et al. Optimal sizing and techno-enviro-economic feasibility assessment of large-scale reverse osmosis desalination powered with hybrid renewable energy sources. *Energy Convers Manage* 2020;224:113377.
- [17] Gökçek M. Integration of hybrid power (wind-photovoltaic-diesel-battery) and seawater reverse osmosis systems for small-scale desalination applications. *Desalination* 2018;435:210–20.
- [18] Peng W, Maleki A, Rosend MA, Azarikhah P. Optimization of a hybrid system for solar-wind-based water desalination by reverse osmosis: Comparison of approaches. *Desalination* 2018;442:16–31.
- [19] Kyriakarakos G, Dounis AI, Arvanitis KG, Papadakis G. Design of a Fuzzy Cognitive Maps variable-load energy management system for autonomous PV-reverse osmosis desalination systems: A simulation survey. *Appl Energy* 2017; 187:575–84.
- [20] Gude VG. Energy storage for desalination processes powered by renewable energy and waste heat sources. *Appl Energy* 2015;137:877–98.
- [21] Moustafa M, Aboulmaaref, Mohamed E, Zayed, Jun Zhao, Wenjia Li, Ahmed A. Askalany, M. Salem Ahmed, et al. Hybrid solar desalination systems driven by parabolic trough and parabolic dish CSP technologies: Technology categorization, thermodynamic performance and economical assessment. *Energy Convers Manage* 2020;220:113103. <http://dx.doi.org/10.1016/j.enconman.2020.113103>.
- [22] Moazeni F, Khazaeei J, Pera-Mendes JP. Maximizing energy efficiency of islanded micro water-energy nexus using co-optimization of water demand and energy consumption. *Appl Energy* 2020;266:114863.
- [23] McManus MC. Environmental consequences of the use of batteries in low carbon systems: The impact of battery production. *Appl Energy* 2012;93:288–95.
- [24] Soshinskaya M, Crijns-Graus WHJ, van der Meer J, Guerrero JM. Application of a microgrid with renewables for a water treatment plant. *Appl Energy* 2014;134: 20–34.
- [25] Carta JA, González J, Subiela V. The SDAWES project: an ambitious R&D prototype for wind-powered desalination. *Desalination* 2004;161:33–48.
- [26] Subiela VJ, Carta JA, González J. The SDAWES project: Lessons learnt from an innovative project. *Desalination* 2004;168:39–47.
- [27] Carta JA, González J, Subiela V. Operational analysis of an innovative wind powered reverse osmosis system installed in the Canary Islands. *Sol Energy* 2003; 75:153–68.
- [28] Carta JA, González J, Cabrera P, Subiela VJ. Preliminary experimental analysis of a small-scale prototype SWRO desalination plant, designed for continuous adjustment of its energy consumption to the widely varying power generated by a stand-alone wind turbine. *Appl Energy* 2015;137:222–39.
- [29] Cabrera P, Folley M, Carta JA. Design and performance simulation comparison of a wave energy-powered and wind-powered modular desalination system. *Desalination* 2021;514:115173.
- [30] Peñate B, Castellano F, Bello A, García-Rodríguez L. Assessment of a stand-alone gradual capacity reverse osmosis desalination plant to adapt to wind power availability: a case study. *Energy* 2011;36:4372–84.
- [31] Loutatidou S, Liosis N, Pohl R, Ouarda TBMJ, Arafat HA. Wind-powered desalination for strategic water storage: Techno-economic assessment of concept. *Desalination* 2017;408:36–53.
- [32] Calise F, Cappiello FL, Vanoli R, Vicidomini M. Economic assessment of renewable energy systems integrating photovoltaic panels, seawater desalination and water storage. *Appl Energy* 2019;253:113575.
- [33] Carta JA, Velázquez S, Cabrera P. A review of measure-correlate-predict (MCP) methods used to estimate long-term wind characteristics at a target site. *Renew Sustain Energy Rev* 2013;27:362–400.
- [34] Karasu S, Altan A. Recognition Model for Solar Radiation Time Series based on Random Forest with Feature Selection Approach. In 2019 11th International Conference on Electrical and Electronics Engineering (ELECO), 2019, p. 8–11. <http://dx.doi.org/10.23919/ELECO47770.2019.8990664>.
- [35] Karasu S, Altan A, Saraç Z, Hacıoğlu R. Estimation of fast varied wind speed based on NARX neural network by using curve fitting. *Int J Energy Appl Technol* 2017;4 (3):137–46.
- [36] Altan A, Karasu S, Zio E. A new hybrid model for wind speed forecasting combining long short-term memory neural network, decomposition methods and grey wolf optimizer. *Appl Soft Comput* 2021;100:106996. <https://doi.org/10.1016/j.asoc.2020.106996>.
- [37] Twidell J, Weir T. *Renewable energy resources*. 3rd ed. New York: Routledge; 2015.
- [38] Cabrera P, Carta JA, González J, Melián G. Artificial neural networks applied to manage the variable operation of a simple seawater reverse osmosis plant. *Desalination* 2017;416:140–56.
- [39] Global Optimization Toolbox User's Guide, The MathWorks, Inc., 2016. Url: http://in.mathworks.com/help/pdf_doc/gads/gads_tb.pdf.
- [40] Deep Kusum, Singh Krishna Pratap, Kansal ML, Mohan C. A real coded genetic algorithm for solving integer and mixed integer optimization problems. *Appl Math Comput* 2009;212(2):505–18.
- [41] Carta JA, Cabrera P, Matías JM, Castellano F. Comparison of feature selection methods using ANNs in MCP-wind speed methods. A case study. *Appl Energy* 2015;158:490–507.
- [42] Díaz S, Carta JA, Matías JM. Comparison of several measure-correlate-predict models using support vector regression techniques to estimate wind power densities. A case study. *Energy Convers Manage* 2017;140:334–54.
- [43] Díaz S, Carta JA, Matías JM. Performance assessment of five MCP models proposed for the estimation of long-term wind turbine power outputs at a target site using three machine learning techniques. *Appl Energy* 2018;209:455–77.
- [44] Hastie T, Tibshirani R, Friedman J. *The elements of statistical learning*. Data Mining, Inference and Prediction. 2nd ed. Springer: Stanford; 2013.
- [45] Cabrera P, Carta JA, González J, Melián G. Wind-driven SWRO desalination prototype with and without batteries: A performance simulation using machine learning models. *Desalination* 2018;435:77–96.
- [46] Breiman L. Random forest. *Mach Learn* 2001;45:5–32.
- [47] Breiman L, Cutler A. *Breiman and Cutler's Random Forests for Classification and Regression*. Package randomForest. Project R Statistics; 2015 [accessed 01.06.2020].
- [48] GNU Project. R Statistics; 2015; Version 3.3.2: <https://www.r-project.org/> [accessed 12 August 2020].
- [49] Karasu S, Altan A, Bekiros S, Ahmad W. A new forecasting model with wrapper-based feature selection approach using multi-objective optimization technique for chaotic crude oil time series. *Energy* 2020;212:118750. <https://doi.org/10.1016/j.energy.2020.118750>.
- [50] Kuhn M. Variable selection using. The Caret Package; 2016. <http://citeseerx.ist.psu.edu/viewdoc/download?doi=10.1.1.168.1655&rep=rep1&type=pdf> [accessed 12 August 2020].
- [51] Kuhn M. Package "caret". Classification and regression training. CRAN R statistics; 2015. <https://github.com/topepo/caret/> [accessed 12 August 2020].
- [52] Willmott CJ, Robeson SM, Matsuura K. A refined index of model performance. *Int J Climatol* 2012;32:2088–94.
- [53] Zhang MH. *Wind resource assessment and micro-siting*. 1st ed. Singapore: Wiley; 2015.
- [54] Pohl R, Kaltschmitt M, Holländer R. Investigation of different operational strategies for the variable operation of a simple reverse osmosis unit. *Desalination* 2009;249:1280–7.
- [55] <http://www.aweo.org/windconsumption.html>.
- [56] Mansour M, Mansouri MN, Mimouni MF. Modeling and Control of IM-based Flywheel Energy-Storage System Associated to a Variable-Speed Wind Generator. In 2ème Conférence Internationale des Energies Renouvelables CIER-2014. Proceedings of Engineering and Technology – PET. http://ipco-co.com/PET_Journal/CIER-2014_Papers/74.pdf.
- [57] <https://ap3.toray.co.jp/toraywater/> [accessed 12 August 2020].
- [58] Papapetroua M, Cipollina A, La Commare U, Micale G, Zaragoza G, Kosmadakis G. Assessment of methodologies and data used to calculate desalination costs. *Desalination* 2017;419:8–19.
- [59] van den Boomen M, Schoenmaker R, Wolfert ARM. A life cycle costing approach for discounting in age and interval replacement optimisation models for civil infrastructure assets. *Struct Infrastruct Eng* 2018;14:1–13.
- [60] Díaz-González F, Sumper A, Gomis-Bellmunt O. *Energy storage in power systems*. 1st ed. Chichester: Wiley; 2016.
- [61] https://www.enercon.de/fileadmin/Redakteur/Medien-Portal/broschueren/pdf/en/ENERCON_Produnkt_en_06_2015.pdf [accessed 13 October 2020].
- [62] <http://www.gobiernodecanarias.org/boc/2018/033/019.html> [accessed 13 October 2020].
- [63] <http://www.gobiernodecanarias.org/boc/2010/204/boc-2010-204-018.pdf> [accessed 13 October 2020].
- [64] <https://www.boe.es/boe/dias/2019/04/17/pdfs/BOE-B-2019-17244.pdf> [accessed 13 October 2020].
- [65] <http://www.gobiernodecanarias.org/boc/2017/008/010.html> [accessed 13 October 2020].
- [66] <http://www.gobiernodecanarias.org/boc/2019/221/018.html> [accessed 13 October 2020].
- [67] <http://www.gobiernodecanarias.org/boc/2018/203/017.html> [accessed 13 October 2020].
- [68] <http://www.gobiernodecanarias.org/boc/2017/058/015.html> [accessed 13 October 2020].
- [69] <https://www.boe.es/boe/dias/2013/03/13/pdfs/BOE-B-2013-9898.pdf> [accessed 07 August 2021].
- [70] <https://www.boe.es/boe/dias/2019/11/14/pdfs/BOE-B-2019-48715.pdf> [accessed 07 August 2021].
- [71] <http://www.gobiernodecanarias.org/boc/2010/234/020.html> [accessed 07 August 2021].
- [72] <https://www.boe.es/boe/dias/2018/02/10/pdfs/BOE-B-2018-8182.pdf> [accessed 07 August 2021].
- [73] <https://www.boe.es/boe/dias/2020/02/10/pdfs/BOE-B-2020-5796.pdf> [accessed 07 August 2021].
- [74] <https://www.boe.es/boe/dias/2020/02/10/pdfs/BOE-B-2020-5797.pdf> [accessed 07 August 2021].
- [75] <http://www.gobiernodecanarias.org/boc/2019/069/022.html> [accessed 07 August 2021].
- [76] <https://www.boe.es/boe/dias/2012/03/13/pdfs/BOE-B-2012-8522.pdf> [accessed 07 August 2021].
- [77] <https://www.boe.es/boe/dias/2018/08/23/pdfs/BOE-B-2018-41222.pdf> [accessed 07 August 2021].
- [78] <https://www.boe.es/boe/dias/2014/02/12/pdfs/BOE-B-2014-5054.pdf> [accessed 07 August 2021].
- [79] <http://www.gobiernodecanarias.org/boc/2012/009/010.html> [accessed 07 August 2021].

- [80] <https://www.boe.es/boe/dias/2013/03/13/pdfs/BOE-B-2013-9899.pdf> [accessed 07 August 2021].
- [81] <http://www.gobiernodecanarias.org/boc/2012/223/018.html> [accessed 07 August 2021].
- [82] <http://www.gobiernodecanarias.org/boc/2019/107/020.html> [accessed 07 August 2021].
- [83] Carta JA, Calero R, Colmenar A, Castro MA, Collado E. Renewable energy power plants. Electricity generation with renewable energies. 2nd ed. Madrid: Pearson; 2012.
- [84] <http://www.desalacion.org/wp-content/uploads/2013/08/OI-12-COSTOS.pdf> [accessed 12 August 2020].
- [85] Voutchkov N. Desalination Engineering Planning and Design. New York: McGraw-Hill; 2013.
- [86] <http://www.agudo.es/perfil-contratante/anuncios-licitacion/obras/1d.pdf> [accessed 12 August 2020].
- [87] <https://www.canalgestionlanzarote.es/wp-content/uploads/2017/04/P.C.-Depo%CC%81sito-Zonzamas-Dic2013-1.pdf> [accessed 12 August 2020].
- [88] Swamee PK, Sharma AK. Design of Water Supply Pipe Networks. New Jersey: Wiley; 2008.
- [89] <https://energystorage.pnnl.gov/pdf/PNNL-28866.pdf>.
- [90] Notton G. Hybrid wind-photovoltaic energy systems. In Sayigh A, editor-in-chief, Kaldellis JK. volume editor. Comprehensive Renewable Energy, vol. 2. Elsevier; 2012, p. 216–53.
- [91] <https://www.caib.es/sacmicrofront/archivopub.do?ctrl=MCRST7085ZI202486&id=202486> [accessed 17 May 2021].
- [92] Velázquez S, Carta JA, Matías JM. Influence of the input layer signals of ANNs on wind power estimation for a target site: A case study. Renew Sustain Energy Rev 2011;15(3). <https://doi.org/10.1016/j.rser.2010.11.036>.
- [93] Carta JA, Díaz S, Castañeda A. A global sensitivity analysis method applied to wind farm power output estimation models. Appl Energy 2020;280:115968.
- [94] Serrano-González J, Lacal-Arántegui R. Technological evolution of onshore wind turbines—a market-based analysis. Wind Energy 2016. <https://doi.org/10.1002/we.1974>.
- [95] Walsh C. Wind energy in Europe in 2019. Trends and statistics. <https://windeurope.org/wp-content/uploads/files/about-wind/statistics/WindEurope-Annual-Statistics-2019.pdf> [accessed 12 August 2021].
- [96] Karagiannis IC, Soldatos PG. Water desalination cost literature: review and assessment. Desalination 2008;223:448–56.
- [97] Riba Esteve. Cálculo y elección óptima de un depósito de agua. <https://upcommons.upc.edu/handle/2099.1/3258> [accessed 12 August 2020].
- [98] Díaz S, Carta JA, Castañeda A. Influence of the variation of meteorological and operational parameters on estimation of the power output of a wind farm with active power control. Renewable Energy 2020;159:812–26.
- [99] Gorissen BL, Yanikoğlu İ, den Hertog D. A practical guide to robust optimization. Omega 2015;53:124–37.
- [100] Prékopa A. Stochastic programming. Springer; 1995.
- [101] Ben-Tal A, El Ghaoui L, Nemirovski A. Robust optimization. Princeton University Press; 2009.
- [102] Cabrera P, Carta JA. Computational Intelligence in the Desalination Industry, Springer. Cham 2019:105–31. https://doi.org/10.1007/978-3-030-25446-9_5.
- [103] Greenlee LF, Lawler DF, Freeman BD, Marrot B. Reverse osmosis desalination: Water Sources, Technology, and Today's Challenges. Water Res 2009;43: 2317–48.
- [104] IRENA. Green hydrogen cost reduction. <https://www.irena.org/publications/2020/Dec/Green-hydrogen-cost-reduction>.
- [105] Ponte B, de la Fuente D, Pino R, Priore P. Multiagent system for intelligent Water Demand Management. In: 2013 International Conference on New Concepts in Smart Cities: Fostering Public and Private Alliances (SmartMILE); 2013. p. 1–7. <https://doi.org/10.1109/SmartMILE.2013.6708195>.
- [106] https://ec.europa.eu/clima/policies/strategies/2050_en.